ANALYSIS FOR STRESSES AND BUCKLING OF

HEATED COMPOSITE STIFFENED PANELS

AND OTHER STRUCTURES

March 1973

By A. V. Viswanathan and M. Tamekuni

ANALYSIS FOR STRESSES AND BUCKLING OF

HEATED COMPOSITE STIFFENED PANELS

AND OTHER STRUCTURES

March 1973

By A. V. Viswanathan and M. Tamekuni

ί

FOREWORD

This work was done under the direction of Dr. Ralph E. Miller, Jr. of The Boeing Company, as the Program Manager and Dr. Michael F. Card of National Aeronautics and Space Administration as the Technical Monitor.

ANALYSIS FOR STRESSES AND BUCKLING OF

HEATED COMPOSITE STIFFENED PANELS

AND OTHER STRUCTURES

by

A. Viswanathan and M. Tamekuni

The Boeing Company, Seattle, Washington

1.0 ABSTRACT

Analytical methods based on linear theory are presented for predicting the thermal stresses in and the buckling of heated structures with arbitrary uniform cross section. The structure is idealized as an assemblage of laminated plate-strip elements, curved and planar, and beam elements. Uniaxially stiffened plates and shells of arbitrary cross section are typical examples. In such structures, the common practice is either to "smear" the stiffeners or to model them as beams along their elastic axis. In contrast, the idealization used here retains the relative stiffnesses and restraints between parts of each stiffener. This may have significant effect on the distribution of thermal stresses and the buckling characteristics. For the buckling analysis the structure or selected elements may be subjected to mechanical loads, in addition to thermal loads, in any desired combination of inplane transverse load and axial compression load. The analysis is also applicable to stiffened structures under inplane loads varying through the cross section, as in stiffened shells under bending. The buckling analysis is general and covers all modes of instability. The analysis has been applied to a limited number of problems and the results are presented. These while showing the validity and the applicability of the method do not reflect its full capability.

iii

2.0 SYMBOLS

a	length of the structure
a_y, b_y, c_y	temperature distribution coefficients, equation (B.3)
A_{ij}	extensional stiffnesses i, j = 1, 2, 6 equation (A.7)
A_b	cross-sectional area of beam element
b	developed width of plate-strip element
B_{ij}	stiffnesses (i, j = 1, 2, 6) associated with coupling between bending and extension, equation (A.8)
C_1	diagonal matrix of longitudinal variables, equations (B.13), (C.4) and (C.5)
$\bar{c}$	transfer matrix, equations (C.11) and (C.12)
d	displacement vector of elements
$\bar{d}$	displacement vector of sub-elements
D	displacement vector of total structure, equations (B.39) and (C.20)
D_{ij}	bending stiffnesses (i, j = 1, 2, 6) equation (A.9)
E_{11}, E_{22}	Young's modulii of orthotropic material
f	force vector of elements
f_A, f_B, f_r	equivalent thermal force vector of plate-strip elements, equations (B.23), (B.28) and (B.21) respectively
$\bar{f}$	force vector of sub-elements
$\bar{f}_b$	equivalent thermal force vector of beam elements, equation (B.34)
$\bar{F}$	equivalent thermal force vector of total structure, equation (B.39)
G_{12}, G_{23}	shear modulii of orthotropic material

h_k	distance to the kth lamina from the reference plane
I_p	polar moment of inertia of beam element
I_{yy}, I_{zz}	moments of inertia of beam element
J	torsion constant for beam element
J_e	effective torsion constant for heated beams, equation (A.56)
k_o, k_A, k_B	diagonal matrices spring constants
k_w, k_θ, k_v, k_u	spring constants
$\bar{K}_o$, $\bar{K}_1$, ... $\bar{K}_8$	coefficients of characteristic equations (B.10)
$\hat{K}_1$, $\hat{K}_2$, ... $\hat{K}_9$	particular solution coefficients, equation (B.7)
ℓ	number of laminas
L_{1i}, L_{2i}	displacement ratio coefficients, equations (B.11)
$\bar{L}_1$, $\bar{L}_2$, ... $\bar{L}_6$	linear differential operators, equations (A.18 to A.23)
m	Fourier coefficient number for thermal stresses and axial half-wave number for buckling, equations (B.2) and (C.3), respectively
M_{11}, M_{12}, M_{22}	moment resultants, equation (A.6)
M_x	torque on the beam element
M_{yT}, M_{zT}	moment resultants in heated beam elements, equations (A.54) and (A.55)
M_{1T}, M_{2T}	moment resultants in heated plate-strip elements, equation (A.11)
$\hat{M}$	moment resultant, equation (A.25)
N_{11}, N_{12}, N_{22}	stress resultants, equation (A.5)
N_{1T}, N_{2T}	force resultants in heated plate-strip elements, equation (A.10)

$\bar{N}_{11}$, $\bar{N}_{22}$	total applied inplane loadings
$\bar{N}_{1m}$, $\bar{N}_{2m}$	applied mechanical inplane loads, equation (C.1) and (C.2)
$\bar{N}_{1p}$, $\bar{N}_{2p}$	applied inplane preloads, equation (C.1) and (C.2)
$\hat{N}$	effective stress resultant in y-direction, equation (A.26)
P_i	displacement parameters, equation (B.6)
$\bar{P}_i$	buckling displacement parameters for sub-elements, equation (C.3)
P	axial load in beam element induced by axial displacements equation (A.52)
P_r	buckling load of plate-strip elements, when the longitudinal (x) sides are completely restrained
P_T	axial load in heated beam element, equation (A.53)
$\bar{P}_b$	applied axial load in beam
q_y, q_z	lateral shears on the beam element equation (A.49) and (A.51)
Q_{ij}	orthotripic material constants (i, j = 1, 2, 6), equation (A.2)
$\hat{Q}$, $\hat{Q}_s$	effective transferse shear parallel to z-axis in plate-strip elements, equations (A.24) and (A.36)
R	reference plane radius of the curved plate-strip element
R_{11}, R_{12}... R_{33}	elements of coefficient matrix R, equation (B.9)
s, $\bar{s}$, s_{11}, s_{12} s_{21}, s_{22}	stiffness matrices for plate-strip elements
s_b	stiffness matrix for beam element

S_A, S_B	reduced stiffness matrices for plate-strip element, equations (B.23), (B.28), (C.17) and (C.18)
S	stiffness matrix of total structure
t_k	thickness of kth layer of a laminate
T, T_x, T_y, T_z	temperature distributions (from ambient conditions)
$\widetilde{T}_o$, $\widetilde{T}_A$, $\widetilde{T}_B$, $\widetilde{T}_b$	transformation matrices
$\hat{T}$	effective inplane shear in plate-strip elements, equation (A.27)
u, v, w	displacements at the reference plane of plate-strip element and at the shear center of beam element
$\bar{u}$, $\bar{v}$, $\bar{w}$	buckling displacements at the reference plane of sub-elements
U_b, V_b, W_b	displacement coefficient for beam element, equation (B.33)
U_i, V_i, W_i	displacement coefficients for plate-strip element, equation (B.6)
$\bar{U}_i$, $\bar{V}_i$, $\bar{W}_i$	buckling displacement coefficients for sub-elements, equation (C.3)
x, y, z	orthogonal coordinates, figures (A.2) and (A.5)
X_1, X_2, X_3, X_4	matrices for plate-strip elements, equations (B.13) to (B.16)
X_5	matrix for beam element defined in equation (B.34)
$\bar{X}_1$, $\bar{X}_2$	matrices for sub-element, equations (C.4), (C.5)
y_o, z_o	plate-strip element offsets, Figure 25
y_m, z_m	distances measured parallel to the y and z axes respectively, from the shear center of the beam element to its neutral axis
α	displacement parameter, equations (B.6) and (C.3)

4

α_{Tx}, α_{Ty}	coefficients of thermal expansion
β_i	displacement parameter, equation (B.6)
$\bar{\beta}_i$	buckling displacement parameter, equation (C.3)
γ_{xy}	shearing strain
Γ	warping constant of beam element
ϵ_x, ϵ_y	normal strains
ζ	angle subtended at its center of curvature by the plate-strip element, Figure 25
θ	rotation or twist
Θ_b	beam twist coefficient, equation (B.33)
$\kappa_x, \kappa_y, \kappa_{xy}$	change in curvatures
$\nu_{12}, \nu_{21},$	Poisson's ratio
σ_x, σ_y	normal stresses
σ_{xy}	shear stress
ϕ, ϕ_A, ϕ_B	transformation angles, equations (A.40) to (A.42)
Ψ	angle between Y_G axis and the chord of plate-strip element, Figure 25

Subscripts

AD	quantities along the side AD of plate-strip element
b	quantities related beam element
BC	quantities along the side BC of plate-strip element
(g)	index for sub-element number
G	quantities related to global axes
i	index corresponding to characteristic roots
k	layer index

5

p   particular solution parts

s   quantities with offset effects

A subscript preceded by a comma indicates partial differentiation
with respect to the subscript.

Superscripts

k   layer index

T   matrix transpose

o   quantities in the reference plane of plate-
                            strip element

+   quantities along the side $y = +\dfrac{b}{2}$ of plate-
                            strip element

−   quantities along the side $y = -\dfrac{b}{2}$ of plate-
                            strip element

3.0 INTRODUCTION

Aerospace vehicles and missiles often operate under severe thermal conditions, thus subjecting the structural components to thermal gradients. The resulting thermal stresses can have significant effects on the characteristics of these structures, Refs. 1, 2 and 3.

Being a self-equilibrating system, the thermal stresses are both tensile and compressive. In thin-walled structures like stiffened plates and shells these stresses reduce the structural performance under mechanical loads and precipitate buckling, Refs. 4 and 5. Thermal stresses can also cause buckling by themselves, if the temperatures are sufficiently high. The usual approach to buckling analysis treats the thermal stresses as pre-loading in conjunction with the established methods of isothermal buckling analyses. Refs. 1 to 6 are typical examples. Thermal stress analysis is thus an essential first step to the proper understanding of the buckling behavior of these structures under combined thermal and mechanical loads.

The analysis of Ref. 7 for buckling under mechanical loads is extended here for thermal stresses and buckling of laminated composite structures of uniform cross section like stiffened panels subjected to these stresses and mechanical loads. As in Ref. 7 the structure is idealized as an assemblage of laminated plate-strip elements, curved and planar, and beam elements. Each element extends the full length of the structure. Element edges normal to the longitudinal axis are assumed to be simply supported with no restriction on the axial (warping) displacement.

The analysis of Ref. 5 is primarily intended for complex shells of revolution. It can also be applied to stiffened panels, retaining the discreteness of the stiffeners, by considering these panels as ring stiffened shells of very large (infinite) radius. Each ring stiffener is treated as a single equivalent beam. Such an idealization is justified when considering the general behavior of complex shells of revolution. However, when applied to stiffened panels the idealization of stiffeners in Ref. 5 is insufficient to predict any local modes of buckling in the stiffeners or any coupled modes involving a contribution from local deformations in the stiffener.

The present analysis enables each stiffener to be idealized as an assemblage of the types of elements mentioned before. Intuitively, this is a better representation of the true behavior of the stiffener. Further, it is possible to distinguish between riveted and bonded connections by means of the modelling techniques discussed in Refs. 7 and 8.

The curved and flat plate-strip elements are in general laminated. Linear or parabolic thermal gradients may be specified across the width of individual elements. An arbitrary thermal gradient through the thickness is approximated by a series of layers, each at a constant temperature. The temperature is constant in the axial direction. The stress-strain equations for each lamina assume orthotropy with respect to the longitudinal and the transverse axes of the element.

Elementary theory of bending and torsion of heated beams under axial loads is used for the beam elements. The section properties of laminated beams are calculated in an approximate manner. Laminated circular and rectangular beam elements are considered in detail. For these, the temperature is arbitrarily constant in each lamina and in the axial direction. For the latter type of beam element, either identically linear or parabolic thermal gradients are allowed across the width of each lamina.

The analysis considers offsets between elements and the effects of arbitrary elastic restraints along any external longitudinal side (i.e., not connected to other elements) of the flat or curved plate-strip elements.

In the thermal stress analysis, a truncated Fourier sine series is used to approximate the constant temperature in the longitudinal direction of each element. Thermal stresses evaluated for each harmonic of the Fourier series are superposed to obtain the resultant thermal stresses corresponding to the boundary conditions discussed before.

The buckling analysis treats the axial thermal load in each beam element as preloads. The above thermal stress resultants, while varying across the width of each plate-strip element, are assumed constant in the longitudinal direction. Because of this transverse variation of the stress resultants, the governing differential equations for each plate-strip element have variable coefficients. Thus, each such element is sub-divided and consequently the variable-coefficient differential equations are reduced, Ref. 9, to corresponding sets of equivalent constant-coefficient differential equations.

The mechanical loading is basically longitudinal compression. However, as in Ref. 7, selected plate-strip elements may also be loaded in the inplane transverse direction. A typical example is biaxially loaded stiffened panels under thermal gradients. In such panels, it is reasonable to assume that the inplane mechanical loading transverse to the stiffener direction is carried entirely by the plate-strip elements in the plane of the skin.

The analyses of thermal stresses and buckling satisfy compatibility on the inter-element boundaries by considering four kinematic degrees of freedom. These correspond to the three translational displacement vectors and the rotational displacement vector about the longitudinal axis. Element stiffness matrices relating the above displacement vectors to the corresponding force vectors on the inter-element boundaries are appropriately merged to yield a set of non-homogenous equations for the thermal stress analysis. For the buckling analysis a similar procedure gives a set of homogeneous equations. The buckling load is obtained by iteratively solving the resulting non-linear eigenvalue problem in a manner analogous to Ref. 7. The eigenvector solution determines the buckling mode shape. The buckling analysis is general and as shown in Ref. 7 yields the lowest buckling load irrespective of the type of buckling.

The basic assumptions in the analysis are:

(a)   The material is linearly elastic. However, the elastic properties corresponding to the average temperature in each lamina may be used.

(b)   Each lamina is orthotropic.

(c)   The Kirchhoff-Love hypothesis is used for the deformation across the thickness.

(d)   Thermo-elastic coupling is ignored.

(e)   Pre-buckling deformations are ignored.

(f)   The edges of each element along $x = 0$ and $x = a$, figures 23 and 26, are simply supported in the classical sense.

The analysis has been coded for the CDC 6600 computer. The computer program "BUCLASP3", (Ref. 10) permits linear or parabolic thermal gradients across the width of individual plate-strip elements. For buckling analysis, the program has an input option whereby the user may also input desired thermal loads as preloads in the structure. The results quoted in this report are from the program "BUCLASP3."

9

4.0 THERMAL STRESS RESULTS

The numerical results from the thermal stress analysis of Appendix B are correlated here with other analytical results. The choice of examples for correlation is restricted by the lack of published results for laminated composite structures including stiffened panels. However, the limited results presented here serve the basic purpose of verifying this analysis and do not reflect its full capability.

The analysis assumes for each element simply supported boundary conditions along the edges normal to the longitudinal axis of the structure. The idealization of the structure as in the present analysis appropriately takes into account the relative internal stiffnesses and restraints which obviously influence the thermal stress distribution. All numerical results from the present analysis quoted below were obtained using the associated computer program "BUCLASP2", Ref. 10.

(i) <u>Isotropic flat panel with two "rod" stiffeners</u>.-Figure 1 shows the geometry of a rectangular isotropic flat panel with two stiffeners. The stiffeners are treated as rods (i.e., they have extensional stiffness only) and are symmetric with respect to the plate. A parabolic thermal gradient corresponding to values of $\alpha_T \Delta T$ of 0.0001 along the sides of the panel and

0.0037 along the line of symmetry, is assumed. The rods are at a constant $\alpha_T \Delta T$ of 0.0033. The results of the present

analysis retaining 16 terms in equation (B.2) are shown in Figure 2 and 3. Plate numbers (1) and (2) refer to the corresponding numbers shown in Figure 1. For comparison the results from a finite element program, Ref. 11, are also shown.

(ii) <u>Isotropic cylinders</u>.-The three isotropic cylinders of Figure 4 have constant temperature rise in the axial direction. The circumferential variation of temperature rise in each case is as indicated in the figure.

The results from the present analysis are shown in Figures 5 to 7. These results were obtained retaining 26 terms in equation (B.2). In Figure 5, the results for cylinder A are shown superposed on the results from Ref. 12. Some discrepancy in the N_{22} value near the ends of the cylinder (x = 0) is noticed. This arises from the fact that in the present analysis, for each Fourier harmonic m in equation (B.2) the corresponding N_{22} has a "sine" distribution in the axial direction. Thus, as the number of harmonics is increased the results of the present analysis in the limit will approach the results of Ref. 12.

For cylinder B, the thermal stress-resultants are shown in Figure 6 superposed on the results from Ref. 13. For both the cylinders A and B the thermal displacements, though not given here, showed excellent correlation.

The results for cylinder C are shown in Figure 7 superposed on the results of Ref. 5.

(iii) Laminated cylinder.-Figure 8 shows a laminated cylinder, each lamina being of a different isotropic material. The laminate has non-zero elements in the coupling matrix B of equations (A.5) and (A.6). The cylinder is subjected to a uniform temperature rise of 400° F. The thermal stress-resultants are shown in Figure 9. The results from the present analysis are obtained retaining 16 terms in equation (B.2). Also shown are the results from Ref. 13. The cause of the discrepancy between the two results near the end of the cylinder (x = 0) is the same as that for the isotropic cylinder A. As the number of terms retained in equation (B.2) is increased the results of the present analysis will converge towards those of Ref. 13.

(iv) Stiffened cylinder-An integrally stiffened cylinder is shown in Figure 10. The stiffeners are idealized as beam elements and the parts of the shell between stiffeners as curved plate-strip elements. For a uniform temperature rise of $\Delta T = 100°$ F, the results of the present thermal analysis retaining 26 terms in equation (B.2), are shown in Figures 11 to 13. Also shown are the results obtained from the computer program "BAMSOC 1" of Ref. 4, using classical analysis. To facilitate comparisons, the results quoted from the present analysis were obtained suppressing the underlined terms in equations (A.4) and (A.12) to (A.14). The analysis of Ref. 4 while taking into account the stiffener eccentricity, "smears" the properties of the stiffener. A similar method is used in Ref. 5. The present analysis not only retains the discreteness of each stiffener but also retains the relative stiffener (especially for other types of stiffeners) using the idealization discussed in Appendix A. The integral stiffeners of the cylinder under discussion were idealized as beam elements purely to conform with Ref. 4. It is more appropriate to idealize these stiffeners as flat plate-strip elements.

The result of the present analysis reflect the effect of the discreteness of the stiffeners. Figure 11 shows the expected change in the out-of-plane displacement w of the shell skin in the region of each stiffener. Similar effects are noticed in the thermal stress distribution in the shell skin shown in Figure 12. The hoop stress N_{22} from the

present analysis is seen to be compressive everywhere in the

cylinder, whereas the results from "BAMSOC 1" show tensile hoop stress in the middle region of the cylinder. This difference is thought to be due to the discreteness of the stiffeners. For the equivalent "smeared" cylinder the present analysis will yield hoop stress distribution as in Figure 5 for the unstiffened cylinder A, this being similar in nature to "BAMSOC 1" results. The peak in N_{22} from the present analysis will move closer and closer to the cylinder end ($x = 0$) together with a simultaneous decrease in the unevenness of N_{22} in the axial direction between $x = 0.5$ and $x = 1.5$, as the number of terms retained in equation (B.2) is increased. Another interesting feature of the results is the presence of the axial stress-resultant N_{11}. For a simply supported cylinder as in this example, analyses based on "smearing" the stiffeners do not predict this stress-resultant. Figure 13 shows the axial load and the bending moment in the integral stiffener.

Similar results may be obtained for cylinders with different types of stiffening and also when circumferential thermal gradients are present.

5.0 BUCKLING RESULTS

Numerical results of the buckling analysis of Appendix C are correlated here with other analytical results. As for the thermal stress results, the choice of examples for correlation is restricted by the lack of published results for heated laminated composite structures. The results presented here are intended to verify the analysis and does not indicate its full capability.

(i) Rectangular flat plates.-Figure 14 shows a series of flat plates under different loading conditions. Each plate is idealized as an assemblage of four plate-strip elements. In plate A and B the only thermal stress is inplane and normal to the x axis. This stress, $\bar{N}_{22}$ is uniform in the plates, thus making it easy to verify the results from the present analysis.

From Ref. 14, the critical value of $\bar{N}_{22}$ for plate A is

1530 lbs/in at m = 1. The corresponding temperature rise

$(\Delta T = \dfrac{\bar{N}_{22}}{E_{11}\alpha_T t})$ is 153°F. The present analysis yields at

at buckling, a temperature rise of 155°F and m = 1.

Plate B is subjected to uniform temperature rise of 35°F and axial mechanical loading $\bar{N}_{11}$. The value of $\bar{N}_{22}$ for

this temperature rise is 350 lbs/in. The critical value of

$\bar{N}_{11}$ from the present analysis is 2338.2 lb/in compared

to 2334.8 lbs/in from Ref. 14 for a biaxially loaded plate with a constant $\bar{N}_{22}$ of 350 lbs/in.

Plate C is subjected to uniform inplane bending as shown in Figure 14. Each plate-strip element is further divided into sub-elements. For a unit bending moment the linearly varying bending stresses are approximated by the corresponding averaged value in each sub-element. These values are increased by a constant factor until the plate buckles. From the present analysis the maximum bending stress-resultant $\bar{N}_{11}$ at buckling is 272.5 lbs/in at m = 2 compared to 271 lbs/in

and the same m value from Ref. 15.

Plate D is subjected to a constant inplane bending corresponding to a maximum stress-resultant $\bar{N}_0$ = 46.885 lb/in

13

with a superposed axial compression of $\bar{N}_{11}$ as in Figure 14

The bending stresses are considered as preloads due to thermal stresses and the axial compression of $\bar{N}_{11}$ is considered as

further mechanical loading. The $\bar{N}_{11}$ at buckling is obtained

as 47.3 lbs/in at m = 2 compared to 46.9 lbs/in, from Ref. 15, at the same m value.

(ii) Isotropic cylinders.-The present buckling analysis assumes the thermal stresses to be invariant in the axial direction. However, as stated in Appendix C, stresses averaged over the length may be used when the axial variation is not too severe. Figure 5 shows the hoop stress resultant N_{22} for

cylinder A of Figure 4. It is seen that N_{22} has a severe variation in the longitudinal (x) direction. Thus, the results from the present analysis can be expected to be very conservative. For this cylinder, Ref. 12 shows that at buckling the maximum value of the compressive hoop stress resultant N_{22} near the end is about 3.44 times the value of

the axially invariant hoop stress resultant causing buckling. Based on the true axial variation of N_{22} , Ref. 12 shows the

temperature rise at buckling for cylinder A to be 2380^{0} F. The present analysis using averaged N_{22} values yields the

critical temperature rise as 740°F. The ratio between these temperatures is 3.22, compared to 3.44 from Ref. 12.

Cylinder C of Figure 4, heated on an axial strip is considered next. The cylinder is idealized by a series of curved plate-strip elements, the elements being considerably narrower in the region of heating. The thermal stress distribution in this cylinder for ΔT_0 = 1°F is shown in Figure 7. For this cylinder, the present buckling analysis gives the critical temperature (ΔT_0)$_{cr}$ = 286° F. The

buckling mode shape is shown in Figure 15. This mode shape agrees with Ref. 5, where as the critical temperature quoted there is (ΔT_0)$_{cr}$ = 194° F. The buckling results of

Ref. 5 is based on treating the cylinder as a portion of a very slender torus. This modelling is equivalent to considering an infinite cylinder, resulting in the thermal stress resultant N_{11} to be constant in the axial direction. In the circumferential direction the value of N_{11} is close

to the "two ring" case shown in Figure 6 of Ref. 5. Thus, the buckling analysis of Ref. 5 in effect approximates the axial

variation of N_{11} in the finite cylinder by its maximum value in the longitudinal direction compared to the averaged value used in the present analysis. Both buckling analyses take into account the circumferential variation of N_{11} . From Ref. 5 the maximum thermal stress resultant N_{11} corresponding to the

temperature rise $(\Delta T_0) = 1° F$,

is 1.3 lbs/in compared to the average value of 0.89 lbs/in from the present analysis. Hence it is reasonable to expect the critical temperatures from the two analyses to be in the inverse ratio of these stress resultants. This in fact is seen to be the case.

The cylinder D shown in Figure 16 is investigated for buckling under pure bending. This is equivalen to a case where the thermal stresses vary in the circumferential direction only. Analytical solutions for such cylinders are given in Refs. 16 and 17.

In the present analysis cylinder D is idealized as a series of curved plate-strip elements which are further divided into sub-elements. These sub-elements being of sufficiently small width, the bending stress in each of them is approximated by an equivalent average stress. These average stresses in each sub-element corresponding to a unit bending moment are input into the computer program "BUCLASP3", Ref. 10. The bending moment is increased in steps proportionately scaling the bending stresses until the cylinder buckles. This is equiva- lent to a thermal buckling problem. The results including the mode shape are shown in Figure 17. The buckling loads are given as the maximum compressive stress resultant N_{11} corres- ponding to the bending moment at buckling. Two sets of results from the present analysis are given. One set corresponds to the complete equations (A.4) and (A.12) to (A.14) while the other set stems from reducting these equations to Donnell-type by suppressing the underlined terms. For comparison, the results from a computer program based on Ref. 18 are also given. The latter is based on Donnell-type equations.

Figure 18 is a plot of the results from the present analysis for the buckling of cylinder D under pure bending to- gether with the results for buckling under uniform axial compression. The range of m-values studied is 1 to 19. As the m-value is increased the buckling load under bending is seen to approach the buckling load under axial compression. These results confirm the conclusions of Refs. 16 and 17.

Similar results may be obtained for cylinders under arbitrarily varying axial and hoop stresses, the variation being confined to the circumferential direction. The cylinders may be of artitrary uniform cross section and may also

be stiffened in the axial direction.

The idealization of the structure as discussed in Appendix A retains the exact discreteness of the stiffeners and enables to determine the lowest of all buckling loads irrespective of whether buckling is of a general nature or is confined to a local region in the stiffener (or shell). The eigenvector solution identifies the true nature of buckling.

(iii) <u>Stiffened cylinder</u>.-Figures 12 and 13 show the thermal stress distribution in the integrally stiffened cylinder of Figure 10. These stresses exhibit severe variation in the axial direction. As discussed earlier, in such cases the present buckling analysis based on the thermal stresses averaged in the axial direction could yield very conservative solutions. Ignoring this for the moment, the stiffened cylinder under consideration is treated as an example where the thermal stresses do not vary in the axial direction, while the variations in the other directions are retained.

The critical temperature rise at buckling from the present analysis is $238.4°F$. The same temperature, on suppressing the underlined terms in equations (A.4) and (A.12) to (A.14), is $247.7 F$. In either case buckling occurs at $n = 1$. Thus, for this cylinder the effects of the additional terms are not very significant, for this particular buckling mode. The mode shape is shown in Figure 19. The stiffeners are seen to enforce buckling nodes in the shell skin. Obviously, the "smearing" of the stiffeners as in Refs. 4 and 5 cannot yield such a buckling mode. For reasons stated in Section 4.0, the stiffeners in the cylinder have been idealized as beam elements. Such an idealization is not capable of yielding any possible local buckling in the stiffeners. This drawback is easily overcome by idealizing the integral stiffeners as flat plate-strip elements. The results for the cylinder under discussion thus brings out the capability of the present analysis in not only retaining the discreteness of the stiffners, but also their true structural characteristics.

(iv) <u>Sheet-stiffener unit</u>.-A titanium sheet-stiffener unit typical of a supersonic airplane wing panel is shown in Figure 20. Here, the thermal gradients corresponding to descent conditions are approximated by constant temperatures in each segment. The axial thermal stress-resultants N_{11} in

in these segments, calculated on the basis of uniform axial strain in the cross section are tabulated in the figure.

The results of two simplified studies illustrating another application of the present analysis to buckling under axial compression load, are given in Figure 21. The riveted connection between the stiffener and the sheet is idealized as

in Refs. 8 and 10. The material properties used in corresponding to the temperature in each segment are given in Figure 20. In the first study, the sides A and B have boundary conditions corresponding to symmetry. The minimum buckling load occurs at m = 1. The resulting mode shape is interesting and shows coupling between Euler, torsional and local modes of buckling. In the second study the sides A and B are simply supported. The minimum buckling load in this case occurs at m = 18 and the corresponding mode shape indicates local buckling in the stiffener web.

It may not be possible to predict the behavior of an entire stiffened panel from such results for an isolated sheet-stiffener unit. This is confirmed by the buckling mode shape for a zee stiffened panel given in Ref. 7.

6.0 CONCLUDING REMARKS

Linear analyses for thermal stresses and buckling of structures of arbitrary uniform cross section have been presented. The structure is idealized as an assemblage of laminated curved plate-strip elements, laminated flat plate-strip elements and beam elements, each element extending the entire length of the structure. The element edges normal to the longitudinal axis are assumed to be simply supported with no restriction on the axial (warping) displacement. The idealization permits differentiating between bonded and riveted connections. The analyses consider the effects of offsets between elements. Longitudinally stiffened panels and shells are typical examples of such structures.

The idealization is seen to represent the true characteristics of these structure in a detailed manner. The relative internal stiffnesses and restraints which obviously influence the thermal stress distribution are appropriately represented unlike the more common method of either smearing the stiffeners or treating them as beams along their elastic axis.

The buckling analysis ignores all pre-buckling deformations and treats the inplane normal thermal stresses as preloads. The preloading is assumed to be constant in each element in the longitudinal direction, while varying across the width of each plate-strip element. Thus the buckling analysis is also applicable to stiffened structures under inplane loads varying through the cross section as in stiffened shells under bending. The theory is general and no assumption is made regarding the buckling mode. The structure is free to take the buckled shape corresponding to minimum energy conditions consistent with prescribed constraints along any external side of plate-strip elements. The eigenvector solution is used to determine the buckled mode shape. The resulting mode shape plot is useful in understanding the buckling mechanism and may be used in efficient design of structures prone to buckling.

The analyses assume that the material is linearly elastic. However, the elastic properties corresponding to the average temperature in each element may be used.

A general lack of other published results makes it difficult to correlate the results from the present analysis. The limited results presented show good correlation.

APPENDIX A

BASIC CONSIDERATIONS

This appendix outlines the basic considerations involved in the analyses of Appendices B and C for thermal stresses and buckling, respectively. A summary of the basic equations used in the analyses are given. These equations are the result of including thermal effects in the basic equations of Ref. 7.

A.1 Idealization of the Structure

Any structure of uniform arbitrary cross section is idealized as an assembly of laminated, curved and planar, plate-strip elements, and beam elements. The beam elements are used to idealize lips and beads in structural sections or any local reinforcement in the form of a lumped area of material. Each element extends the full length of the structure. The intersecting angle between elements is arbitrary. Element edges normal to the longitudinal axis are assumed to be simply supported with no restriction on the axial (warping) displacement. Arbitrary elastic restraint boundary conditions may be specified along any external longitudinal side (not connected to other elements) of flat and curved plate-strip elements.

Figure 22 shows the uniform cross section of an arbitrary structure. The longitudinal (x) sides along G and H are arbitrarily restrained. This structure is idealized as an assemblage of:

    (a)   Curved plate-strip elements: 2, 3 and 9

    (b)   Flat plate-strip elements: 1, 4, 5, 7, 8, and 11

    (c)   Beam elements : 6 and 10

In this figure the element numbers are shown circled. Each plate-strip element is considered replaced by a membrane in its mid-plane (chosen as the reference plane). Each beam element is considered replaced by a line through its shear center. The broken line shown is drawn through the mid-plane of each plate-strip element. The extremities of the individual mid-planes and the shear center of each beam element are marked with "dots." x_G, y_G and z_G are

the chosen global axes; x_G being parallel to the longitudinal

axis of the structure. y and z are the local axes in each element. The local x axis (not shown in the figure) is parallel to x_G. The idealization of the

structure, as indicated above, also defines any offsets between elements. It is possible to differentiate between bonded and riveted connections as discussed in Ref. 10.

A.2 Laminated Curved and Flat Plates

The equations given here are for the laminated curved plate. They degenerate to those of the laminated flat plate when the curvature becomes zero (infinite radius).

Figure 23 shows the geometry and sign conventions for the curved laminate. The x, y and z axes are assumed coincident with the fiber axes 1, 2, and 3. The mid-plane of the laminate is chosen as the reference plane. The stress-strain equations for an orthotropic lamina with a temperature change T from ambient conditions (in the unstressed state T = 0) are, Ref. 19:

$$
\begin{Bmatrix} \sigma_x^k \\ \sigma_y^k \\ \sigma_{xy}^k \end{Bmatrix} = \begin{bmatrix} Q_{11}^k & Q_{12}^k & 0 \\ Q_{12}^k & Q_{22}^k & 0 \\ 0 & 0 & Q_{66}^k \end{bmatrix} \begin{Bmatrix} \epsilon_x - \alpha_{Tx}^k T \\ \epsilon_y - \alpha_{Ty}^k T \\ \gamma_{xy} \end{Bmatrix}
\qquad (A.1)
$$

Where the superscript k identifies the lamina member and

$$
Q_{11}^k = \frac{E_{11}}{(1 - \nu_{12}\nu_{21})}
$$

$$
Q_{22}^k = \frac{E_{22}}{(1 - \nu_{12}\nu_{21})}
$$

$$
Q_{12}^k = \frac{\nu_{21}E_{11}}{(1 - \nu_{12}\nu_{21})} = \frac{\nu_{12}E_{22}}{(1 - \nu_{12}\nu_{21})}
\qquad (A.2)
$$

$$
Q_{66}^k = G_{12}
$$

α_{Tx}^{k} and α_{Ty}^{k} are the coefficients of thermal expansion of the kth layer in the two orthogonal direction x and y, respectively.

Based on the Kirchhoff-Love hypothesis, the strains in any plane at distance z from the reference plane are:

$$\left\{ \begin{array}{c} \epsilon_x \\ \epsilon_y \\ \gamma_{xy} \end{array} \right\} = \left\{ \begin{array}{c} \epsilon_x^{\circ} \\ \epsilon_y^{\circ} \\ \gamma_{xy}^{\circ} \end{array} \right\} + z \cdot \left\{ \begin{array}{c} \kappa_x^{\circ} \\ \kappa_y^{\circ} \\ \kappa_{xy}^{\circ} \end{array} \right\} \tag{A.3}$$

ϵ_x° , ϵ_y° , and ϵ_{xy}° are the strains and κ_x° , κ_y° and κ_{xy}° are the changes in curvature of the reference surface. From Ref. 20, these are written in terms of the corresponding displacements u, v and w, as:

$$\epsilon_x^{\circ} = u_{,x}$$

$$\epsilon_y^{\circ} = v_{,y} - \frac{w}{R}$$

$$\gamma_{xy}^{\circ} = u_{,y} + v_{,x}$$

$$\kappa_x^{\circ} = -w_{,xx}$$

$$\kappa_y^{\circ} = -w_{,yy} - \frac{1}{R} v_{,y}$$

$$\kappa_{xy}^{\circ} = -2w_{,xy} - \frac{2}{R} v_{,x}$$

(A.4)

The above equations reduce to the Donnell-type assumptions when the underlined terms are dropped.

21

Combining equations (A.1), (A.3), and (A.4) and integrating over the thickness of the laminate, the stress resultants and the moment resultants in the reference plane are:

$$
\begin{Bmatrix} N_{11} \\ N_{22} \\ N_{12} \end{Bmatrix} = \begin{bmatrix} A_{11} & A_{12} & 0 \\ A_{12} & A_{22} & 0 \\ 0 & 0 & A_{66} \end{bmatrix} \begin{Bmatrix} \epsilon_x^{\circ} \\ \epsilon_y^{\circ} \\ \gamma_{xy}^{\circ} \end{Bmatrix} + \begin{bmatrix} B_{11} & B_{12} & 0 \\ B_{12} & B_{22} & 0 \\ 0 & 0 & B_{66} \end{bmatrix} \begin{Bmatrix} \kappa_x^{\circ} \\ \kappa_y^{\circ} \\ \kappa_{xy}^{\circ} \end{Bmatrix} - \begin{Bmatrix} N_{1T} \\ N_{2T} \\ 0 \end{Bmatrix} \quad (A.5)
$$

$$
\begin{Bmatrix} M_{11} \\ M_{22} \\ M_{12} \end{Bmatrix} = \begin{bmatrix} B_{11} & B_{12} & 0 \\ B_{12} & B_{22} & 0 \\ 0 & 0 & B_{66} \end{bmatrix} \begin{Bmatrix} \epsilon_x^{\circ} \\ \epsilon_y^{\circ} \\ \gamma_{xy}^{\circ} \end{Bmatrix} + \begin{bmatrix} D_{11} & D_{12} & 0 \\ D_{12} & D_{22} & 0 \\ 0 & 0 & D_{66} \end{bmatrix} \begin{Bmatrix} \kappa_x^{\circ} \\ \kappa_y^{\circ} \\ \kappa_{xy}^{\circ} \end{Bmatrix} - \begin{Bmatrix} M_{1T} \\ M_{2T} \\ 0 \end{Bmatrix} \quad (A.6)
$$

where

$$
A_{ij} = \sum_{k=1}^{\ell} Q_{ij}^{k} t^{k} \quad (A.7)
$$

$$
B_{ij} = \frac{1}{2} \sum_{k=1}^{\ell} Q_{ij}^{k} (h_{k+1} + h_k) \, t_k \quad (A.8)
$$

$$
D_{ij} = \frac{1}{3} \sum_{k=1}^{\ell} Q_{ij}^{k} (h_{k+1}^2 + h_{k+1} \cdot h_k + h_k^2) \, t_k \quad (A.9)
$$

$$(i, j = 1, 2, 6)$$

$$
\begin{Bmatrix} N_{1T} \\ N_{2T} \end{Bmatrix} = \sum_{k=1}^{\ell} \int_{h_k}^{h_{k+1}} \begin{bmatrix} Q_{11}^{k} & Q_{12}^{k} \\ Q_{12}^{k} & Q_{22}^{k} \end{bmatrix} \begin{Bmatrix} \alpha_{Tx}^{k} \\ \alpha_{Ty}^{k} \end{Bmatrix} \cdot T \cdot dz \quad (A.10)
$$

$$
\begin{Bmatrix} M_{1T} \\ M_{2T} \end{Bmatrix} = \sum_{k=1}^{\ell} \int_{h_k}^{h_{k+1}} \begin{bmatrix} Q_{11}^{k} & Q_{12}^{k} \\ Q_{12}^{k} & Q_{22}^{k} \end{bmatrix} \begin{Bmatrix} \alpha_{Tz}^{k} \\ \alpha_{Ty}^{k} \end{Bmatrix} \cdot T \cdot z \cdot dz \quad (A.11)
$$

h_k and h_{k+1} are the distances to the upper and lower surfaces, respectively, of the kth lamina. The A, B and D coefficient matrices define the overall extensional, coupling and bending stiffnesses, respectively, of the laminate, in relation to the chosen reference plane (here, the mid-plane). The thermal terms are shown with an additional subscript T.

Suitable "stability equations" and consistent boundary conditions for the laminated curved plate under external biaxial mechanical loads, $\bar{N}_{11}$ and $\bar{N}_{22}$, are derived in Ref. 7, ignoring pre-buckling deformations. The equations are:

$$N_{11,x} + N_{12,y} - \bar{N}_{11}\, u,_{xx} - \bar{N}_{22}\, u,_{yy} = 0 \tag{A.12}$$

$$N_{22,y} + N_{12,x} - \frac{1}{R}\,(M_{22,y} + 2M_{12,x}) - \bar{N}_{11}\, v,_{xx}$$

$$- \bar{N}_{22}\left(v,_{yy} - \frac{2}{R}\, w,_y - \frac{1}{R^2}\, v\right) = 0 \tag{A.13}$$

$$M_{11,xx} + M_{22,yy} + 2M_{12,xy} + \frac{1}{R}\, N_{22} - \bar{N}_{11}\, w,_{xx}$$

$$- \bar{N}_{22}\left(\frac{2}{R}\, v,_y + w,_{yy} - \frac{1}{R^2}\, w\right) = 0 \tag{A.14}$$

After substituting equations (A.4) to (A.6), the above equations are written as:

$$\bar{L}_1\, u + \bar{L}_2\, v + \bar{L}_3\, w = N_{1T,x} \tag{A.15}$$

$$\bar{L}_2\, u + \bar{L}_4\, v + \bar{L}_5\, w = N_{2T,y} - \frac{M_{2T,y}}{R} \tag{A.16}$$

$$\bar{L}_3\, u + \bar{L}_5\, v + \bar{L}_6\, w = -\frac{N_{2T}}{R} - M_{1T,xx} - M_{2T,yy} \tag{A.17}$$

where the linear differential operators $\bar{L}_1$ to $\bar{L}_6$ are defined by:

$$\bar{L}_1 = A_{11}\,(\ ),_{xx} + A_{66}\,(\ ),_{yy} - \bar{N}_{11}\,(\ ),_{xx} - \bar{N}_{22}\,(\ ),_{yy} \tag{A.18}$$

$$\bar{L}_2 = (A_{12} + A_{66})\,(\ ),_{xy} - \frac{1}{R}\,(B_{12} + 2B_{66})\,(\ ),_{xy} \tag{A.19}$$

$$\bar{L}_3 = -B_{11}\,(\ ),_{xxx} - (B_{12} + 2B_{66})\,(\ ),_{xyy} - \frac{A_{12}}{R}\,(\ ),_x \tag{A.20}$$

$$\bar{L}_4 = A_{22}\,(\ ),_{yy} + A_{66}\,(\ ),_{xx} + \left(\frac{4D_{66}}{R^2} - \frac{4B_{66}}{R}\right)(\ ),_{xx}$$

$$+ \left(\frac{D_{22}}{R^2} - \frac{2B_{22}}{R}\right)(\ ),_{yy} - \bar{N}_{11}\,(\ ),_{xx} - \bar{N}_{22}\,(\ ),_{yy} - \frac{\bar{N}_{22}}{R^2}\,(\ ) \tag{A.21}$$

$$\bar{L}_5 = -(B_{12} + 2B_{66})(\ )_{,xxy} - B_{22}(\ )_{,yyy} - \frac{A_{22}}{R}(\ )_{,y} + \frac{B_{22}}{R^2}(\ )_{,y}$$

$$+ \frac{1}{R}(4D_{66} + D_{12})(\ )_{,xxy} + \frac{D_{22}}{R}(\ )_{,yyy} - \frac{2\bar{N}_{22}}{R}(\ )_{,y} \tag{A.22}$$

$$\bar{L}_6 = D_{11}(\ )_{,xxxx} + (2D_{12} + 4D_{66})(\ )_{,xxyy} + D_{22}(\ )_{,yyyy}$$

$$+ \frac{2B_{12}}{R}(\ )_{,xx} + \frac{2B_{22}}{R}(\ )_{,yy} + \frac{A_{22}}{R^2}(\ ) + \bar{N}_{11}(\ )_{,xx} \tag{A.23}$$

$$+ \bar{N}_{22}(\ )_{,yy} - \frac{\bar{N}_{22}}{R^2}(\ )$$

The boundary conditions along any side $y = $ constant are:

$$w = 0 \qquad \text{or} \qquad \hat{Q} = M_{22,y} + 2M_{12,x} - \bar{N}_{22}\left(\frac{v}{R} + w_{,y}\right) = 0 \tag{A.24}$$

$$\theta = \left(w_{,y} + \frac{v}{R}\right) = 0 \qquad \text{or} \qquad \hat{M} = M_{22} = 0 \tag{A.25}$$

$$v = 0 \qquad \text{or} \qquad \hat{N} = N_{22} - \bar{N}_{22}\left(v_{,y} - \frac{w}{R}\right) = 0 \tag{A.26}$$

$$u = 0 \qquad \text{or} \qquad \hat{T} = N_{12} - \bar{N}_{22}\,u_{,y} = 0 \tag{A.27}$$

Similarly, along any edge $x = $ constant:

$$w = 0 \qquad \text{or} \qquad \tilde{Q} = M_{11,x} + 2M_{12,xy} - \bar{N}_{11}w_{,x} = 0 \tag{A.28}$$

$$w_{,x} = 0 \qquad \text{or} \qquad \tilde{M} = M_{11} = 0 \tag{A.29}$$

$$v = 0 \qquad \text{or} \qquad \tilde{T} = N_{12} - \bar{N}_{11}\,v_{,x} = 0 \tag{A.30}$$

$$u = 0 \qquad \text{or} \qquad \tilde{N} = N_{11} - \bar{N}_{11}\,u_{,x} = 0 \tag{A.31}$$

$\hat{Q}$, $\tilde{Q}$, etc., are the effective force resultants along the sides and edges of the plate-strip element. The above equations (A.12) to (A.31) reduce to Donnell-type equations for thin cylindrical shells when the underlined terms are dropped. Further, when the external mechanical loads $\bar{N}_{11}$ and $\bar{N}_{22}$ are zero, the above equations are identical to the equilibrium equations and the boundary conditions for thermal stress analysis.

The displacements and forces in equations (A.24) to (A.31) are mid-plane values (chosen as the reference plane) and are with respect to the local axes. The positive directions of such displacements and forces along the sides $y = +\dfrac{b}{2}$ and $y = -\dfrac{b}{2}$ of the plate-strip element are shown in Figure 24. Later, in Appendices B and C it will be necessary to transform these to parallel offset planes and also to global axes which make an arbitrary angle with the local axes. These transformations are discussed in Ref. 7 and are outlined below.

Figure 25 shows a plate-strip element ABCD in relation to arbitrarily chosen global axes x_G, y_G and z_G. Also shown are typical offsets to S, for the side BC. Axes system x_S, y_S and z_S at S are chosen parallel to the local axes at B. The offsets are defined by the distances y_0 and z_0 measured positive along the positive local y and z axes, respectively, from the side of the plate-strip element in the reference plane. The displacements and forces in equations (A.24) to (A.27) are transformed to the axes system through S as:

$$w_S = w + y_0\,\theta \tag{A.32}$$

$$\theta_S = \theta \tag{A.33}$$

$$v_S = v - z_0 \cdot \theta \tag{A.34}$$

$$u_S = u - z_0 \cdot w_{,x} - y_0 \cdot v_{,x} \tag{A.35}$$

$$\hat{Q}_S = \hat{Q} - z_0\,\hat{T}_{,x} \tag{A.36}$$

$$\hat{M}_S = \hat{M} + y_0 \cdot \hat{Q} - z_0 \cdot \hat{N} \tag{A.37}$$

$$\hat{N}_S = \hat{N} - y_0 \cdot \hat{T}_{,x} \tag{A.38}$$

$$\hat{T}_S = \hat{T} \tag{A.39}$$

Figure 25 also shows positive directions of the global displacements and forces, subscripted G. From geometry, it is seen that the transformation angle to global axes at A is:

$$\phi_A = \psi - \frac{\zeta}{2} \tag{A.40}$$

and at B

$$\phi_B = \psi + \frac{\zeta}{2} \tag{A.41}$$

The angle is measured positive in the clockwise direction, from the global axes. For a flat plate-strip element

$$\phi_A = \phi_B = \psi$$

A matrix $\widetilde{T}_o$ for coordinate transformation through angle   is defined as:

$$\widetilde{T}_o = \begin{bmatrix} \cos\phi & 0 & \sin\phi & 0 \\ 0 & 1 & 0 & 0 \\ -\sin\phi & 0 & \cos\phi & 0 \\ 0 & 0 & 0 & 1 \end{bmatrix} \tag{A.42}$$

Also defining displacement and force vectors as:

$$d_s = [w_s, \theta_s, v_s, u_s]^T \tag{A.43}$$

$$d_G = [w_G, \theta_G, v_G, u_G]^T \tag{A.44}$$

$$f_s = [\hat{Q}_s, -\hat{M}_s, \hat{N}_s, \hat{T}_s]^T \tag{A.45}$$

$$f_G = [\hat{Q}_G, \hat{M}_G, \hat{N}_G, \hat{T}_G]^T \tag{A.46}$$

and using superscripts - and + to denote the two sides of the plate-strip element identified by the values of $y = -\frac{b}{2}$ and $y = +\frac{b}{2}$, respectively, the displacements and

forces in equations (A.32) to (A.39) are transformed to global axes as:

$$
\begin{Bmatrix} d_G^- \\ d_G^+ \end{Bmatrix} = \begin{bmatrix} \tilde{T}_A & 0 \\ 0 & \tilde{T}_B \end{bmatrix} \begin{Bmatrix} d_s^- \\ d_s^+ \end{Bmatrix}
\tag{A.47}
$$

$$
\begin{Bmatrix} f_G^- \\ f_G^+ \end{Bmatrix} = \begin{bmatrix} -\tilde{T}_A & 0 \\ 0 & \tilde{T}_B \end{bmatrix} \begin{Bmatrix} f_s^- \\ f_s^+ \end{Bmatrix}
\tag{A.48}
$$

$\tilde{T}_A$ and $\tilde{T}_B$ are the coordinate transformation matrices obtained from equation (A.42) for angles ϕ_A of equation (A.40) and of equation (A.41), respectively. The negative sign associated with $\hat{M}_s$ in equation (A.45) facilitates the use of a common coordination transformation matrix. The negative sign associated with $\tilde{T}_A$ in equation (A.48) is a consequence of the sign convention for forces in the local axis system.

A.3 Laminated Beams

Concentrated local reinforcements, like beads or lips in stiffeners, corner fillets in extruded sections, any beam type boron reinforcements, etc., are idealized as beam elements. Figure 26 shows the geometry and sign conventions for these elements. Any beam element is idealized as a line in the longitudinal (x) direction through its shear center.

The general theory, Ref. 1, for beams subjected to a temperature change T and axial load $\bar{P}_b$, gives the following equations:

$$
q_z = E_{11}I_{yy} \frac{d^4 w}{dx^4} + \bar{P}_b \frac{d^2 w}{dx^2} + \bar{P}_b y_m \frac{d^2 \theta}{dx^2} + \frac{d^2 M_{yT}}{dx^2}
\tag{A.49}
$$

$$\frac{dM_x}{dx} = E_{11}\Gamma \frac{d^4\theta}{dx^4} + (\bar{\sigma}I_p - G_{23}J_e)\frac{d^2\theta}{dx^2} + \bar{P}_b y_m \frac{d^2w}{dx^2} - \bar{P}_b z_m \frac{d^2v}{dx^2} \qquad (A.50)$$

$$q_y = E_{11}I_{zz}\frac{d^4v}{dx^4} + \bar{P}_b \frac{d^2v}{dx^2} - \bar{P}_b z_m \frac{d^2\theta}{dx^2} + \frac{d^2M_{zT}}{dx^2} \qquad (A.51)$$

$$\frac{dP}{dx} = -E_{11}A_b \frac{d^2u}{dx^2} + \frac{dP_T}{dx} \qquad (A.52)$$

The thermal terms shown with the additional subscript T are given by:

$$P_T = \sum_{k=1}^{\ell} \int_{A_b^k} \alpha_T^k E_{11}^k T^k dA_b^k \qquad (A.53)$$

$$M_{yT} = \sum_{k=1}^{\ell} \int_{A_b^k} \alpha_T^k E_{11}^k T^k \bar{z} \, dA_b^k \qquad (A.54)$$

$$M_{zT} = \sum_{k=1}^{\ell} \int_{A_b^k} \alpha_T^k E_{11}^k T^k \bar{y} \, dA_b^k \qquad (A.55)$$

where $\bar{y} = (y - y_m)$ and $\bar{z} = (z - z_m)$

The effective torsional stiffness $G_{23}J_e$ is given by

$$G_{23}J_e = G_{23}J + \sum_{k=1}^{\ell} \int_{A_b^k} \sigma_{xT} (\bar{y}^2 + \bar{z}^2) \, dA_b^k \qquad (A.56)$$

The second term on the right-hand side of equation (A.56) represents the thermal effect on torsional stiffness. The presence of the term can either decrease or increase the effective torsional stiffness, though generally a decrease will occur. This is discussed in Refs. 1, 21, and 22.

The positive directions of the displacements u, v, and w and the twist θ of the beam element are shown in Figure 26. y_m and z_m are the distances measured parallel to the principal axes y and z, respectively, from the shear center 0 to the neutral axis C. These distances are positive in the positive directions of the axes. Approximate methods to evaluate the gross beam properties $E_{11}I_{yy}$, $E_{11}I_{zz}$, $E_{11}\Gamma$, $\bar{\sigma}I_p$, $G_{23}J$

and $E_{11}A_b$ for the more common beam types, namely the laminated rectangular and the laminated circular beam elements are given in Ref. 7.

Some limitations of the above equations for the heated beam element are discussed in Ref. 23. However, the equations given are considered to be sufficiently accurate for the envisaged applications of the beam element, mentioned at the beginning of this sub-section.

An offset transformation identical to that for the plate-strip elements, equations (A.32) to (A.39) can be readily done. However, it is not pursued here as the offsets in plate-strip elements would suffice for the idealization of the types of structures considered. The beam element displacements and corresponding forces may be transformed to global axes oriented at an angle ϕ_b measured clockwise from the global axes to the local axes. Thus,

$$d_{bG} = \widetilde{T}_b\, d_b \tag{A.57}$$

$$f_{bG} = \widetilde{T}_b\, f_b \tag{A.58}$$

where

$$d_b = [w,\ \theta,\ v,\ u]^T \tag{A.59}$$

$$f_b = \left[q_z,\ \frac{dM_x}{dx},\ q_y,\ \frac{dP}{dx} \right]^T \tag{A.60}$$

d_{bG} and f_{bG} are the global displacement and force vectors, defined in equations (A.44) and (A.46). $\widetilde{T}_b$ is the coordinate transformation matrix of equation (A.42), for the angle ϕ_b.

APPENDIX B

THERMAL STRESS ANALYSIS

The equations of Appendix A are now used in developing an analysis for thermal stresses in structures of uniform cross section. The structure is idealized as discussed in sub-section A.1.

For each plate-strip elements, linear or parabolic thermal gradients may be specified across the width. An arbitrary thermal gradient through the thickness is approximated by a series of layers, each at constant temperature. Temperature is constant in the longitudinal (x) direction. For the laminated circular and rectangular beam elements the temperature is arbitrarily constant in each lamina and in the longitudinal direction. For the latter type of beam element, identically linear or parabolic thermal gradients are allowed across the width of each lamina. The equations of sub-section A.3 are applicable to any arbitrary beam element, provided the necessary beam properties are known.

The material of the structure is assumed to be linearly elastic. However, the elastic properties corresponding to the average temperature in each lamina may be used.

The constant temperatures in the axial direction of each element are approximated by a truncated Fourier sine series. The governing differential equations for each type of element are satisfied in an exact manner. Then, the stiffness matrices for these elements, relating the forces and displacements along inter-element boundaries, are derived taking into account the effects of thermal gradients.

For each harmonic of the Fourier series, the element stiffness matrices are merged in a manner analogous to the direct stiffness method of finite element analysis. The axial (x) variations of the various quantities are separated out. The resulting non-homogeneous equations are solved for the thermal displacements using the symmetric Gaussian elimination algorithm. The displacements yield the thermal strains and stresses. Solutions are obtained in a similar manner for each haromonic and the results are superposed to yield the resultant thermal stresses.

5.1 Stiffness of Heated Curved and Flat Plate-Strip Elements

In a laminated curved or flat plate-strip elements, the temperature change from ambient conditions are specified as:

$$T = T_x \ T_y \ T_z \tag{B.1}$$

Since the thermal field in the axial (x) direction, Figure 23, is assumed not to vary, T_x is a constant for each plate-strip element and is approximated by the truncated Fourier series:

$$T_x = T_x \cdot \sum_{m=1,3,5\ldots} \frac{4}{m\pi} \sin \frac{m\pi x}{a} \qquad (B.2)$$

In the transverse (y) direction the thermal field is assumed as:

$$T_y = a_y + b_y \cdot y + c_y \cdot y^2 \qquad (B.3)$$

In the thickness direction (z), the thermal gradient may be arbitrary and is approximated by a series of layers each at a constant temperature. Thus the temperature distribution in the kth layer is given by:

$$T^k = T_x \cdot T_y \cdot T_z^{\,k}$$

Equations are now developed for the stiffness matrix relating the thermal displacements and the corresponding forces along the sides $y = \pm \frac{b}{2}$ of the laminated curved plate-strip element. In the limit as the curvature becomes zero (infinite radius), these equations degenerate to those of the flat plate-strip element. The displacements considered are:

$$w, \quad \theta = \left(w_{,y} + \frac{v}{R} \right), \text{ v and u} \qquad (B.4)$$

The corresponding forces are, from equations (A.24) to (A.27):

$$\hat{Q} = M_{22,y} + 2M_{12,x}$$

$$\hat{M} = M_{22}$$

$$\hat{N} = N_{22} \qquad (B.5)$$

$$\hat{T} = N_{12}$$

Since the thermal stresses are being considered, all terms involving the external mechanical loads $\bar{N}_{11}$ and $\bar{N}_{22}$ have been dropped. The positive directions of the above displacements and forces are shown in Figure 24. The governing differential equations (A.23) to (A.25) for the plate-strip element are non-homogeneous. For each harmonic, m, in the equation (B.2), the complementary solution is assumed as:

$$w_c = \sum_{i=1}^{8} W_i \, e^{\beta_i} \sin \alpha$$

$$v_c = \sum_{i=1}^{8} V_i \, e^{\beta_i} \sin \alpha \qquad\qquad (B.6)$$

$$u_c = \sum_{i=1}^{8} U_i \, e^{\beta_i} \cos \alpha$$

where $\quad \alpha = \dfrac{m\pi x}{a}$ and $\beta_i = \dfrac{p_i \pi y}{a}$

p_i $(i = 1, 2, \ldots 8)$ are the roots of the characteristic

equation, discussed later. The corresponding particular solution is assumed as:

$$w_p = \left(\hat{K}_7 + \hat{K}_8 y + \hat{K}_9 y^2\right) \sin \alpha$$

$$v_p = \left(\hat{K}_4 + \hat{K}_5 y + \hat{K}_6 y^2\right) \sin \alpha \qquad\qquad (B.7)$$

$$u_p = \left(\hat{K}_1 + \hat{K}_2 y + \hat{K}_3 y^2\right) \cos \alpha$$

The above displacement functions are chosen to satisfy ab initio the simply supported boundary conditions defined by:

$$w = M_{11} = v = N_{11} = 0 \qquad\qquad (B.8)$$

along the edges $x = 0$ and $x = a$. For the complementary
solution, a typical term of equation (B.6) is substituted into
equations (A.15) to (A.17) and setting the right-hand sides to
zero, results in:

$$
\begin{bmatrix}
R_{11} & R_{12} & \pi R_{13} \\
R_{21} & R_{22} & \pi R_{23} \\
R_{31} & R_{32} & \pi R_{33}
\end{bmatrix}
\begin{Bmatrix}
U_i \\
V_i \\
W_i
\end{Bmatrix} = 0
\tag{B.9}
$$

Expressions for the R_{ij} coefficients $(i, j = 1, 2, 3)$ may be
readily derived from equations (A.18) to (A.23), after dropping
all terms in $\bar{N}_{11}$ and $\bar{N}_{22}$. On expanding the determinant of
the coefficient matrix in equation (B.9), a characteristic
polynomial is obtained as:

$$
\bar{K}_8 p_i^8 + \bar{K}_6 p_i^6 + \bar{K}_4 p_i^4 + \bar{K}_2 p_i^2 + \bar{K}_0 = 0
\tag{B.10}
$$

This equation yields eight values of p_i which are real or
complex conjugates. Four of these roots are the negatives of
the other four. Also, from equation (B.9)

$$
U_i = \pi L_{2i} W_i
$$
$$
V_i = \pi L_{1i} W_i
\tag{B.11}
$$

$$
L_{1i} = \frac{R_{23} R_{11} - R_{13} R_{21}}{R_{12} R_{21} - R_{22} R_{11}}
$$

$$
L_{2i} = \frac{R_{13} R_{22} - R_{23} R_{12}}{R_{12} R_{21} - R_{22} R_{11}}
\tag{B.12}
$$

$$
(i = 1, 2, \ldots \ldots 8)
$$

33

The complementary displacement functions of equation (B.6) are now fully defined for each harmonic, m, except for the amplitude coefficients W_i. The contributions of these functions to the "complete" displacements and the corresponding "complete" forces of equations (B.4) and (B.5) may be readily calculated in terms of W_i. The procedure is analogous to that in Appendix B of Ref. 7.

Next, the $\hat{K}_i$ coefficients (i = 1, 2, ...9) in the particular solution functions of equation (B.7) are determined from equations (A.15) to (A.17) by the usual method for non-homogeneous differential equations. The right-hand sides in these equations contain all the thermal terms and are evaluated using equations (A.10) and (A.11). The above procedure yields explicit expressions for the $\hat{K}_i$ coefficients.

The details, though not given here, will result in all $\hat{K}_i$ coefficients except $\hat{K}_6$ being non-zero. The particular solution functions are now fully defined. Thus, the contributions of the particular solution functions to the "complete" displacements and the corresponding "complete" forces of equations (B.4) and (B.5) are explicitly known.

Finally, the complementary solution results, in terms of the yet unknown amplitude coefficients W_1, and the explicitly known particular solution results are superimposed to yield the "complete" displacements and the "complete" forces for each harmonic, m, in equation (B.2).

In idealizing a structure as discussed in Appendix A offsets between elements may occur. Further, the intersecting angle between elements being arbitrary, it is convenient to transform all displacements and forces to common global axes. The necessary transformations have been outlined in Appendix A. Following the procedure of Ref. 7, such transformations yield the following equations for the displacements and forces along the sides $y = -\frac{b}{2}$ and $y = +\frac{b}{2}$ of the plate-strip element:

$$\begin{Bmatrix} d_G^- \\ d_G^+ \end{Bmatrix} = \begin{bmatrix} \tilde{T}_A & 0 \\ 0 & \tilde{T}_B \end{bmatrix} \begin{bmatrix} C_1 X_1^- \\ C_1 X_1^+ \end{bmatrix} \{W_i\} + \begin{Bmatrix} d_p^- \\ d_p^+ \end{Bmatrix} \qquad \text{(B.13)}$$

or

$$d_G = C_2 X_3 W_i + d_{pG} \qquad \text{(B.14)}$$

$$\begin{Bmatrix} f_G^- \\ f_G^+ \end{Bmatrix} = \begin{bmatrix} -\tilde{T}_A & 0 \\ 0 & \tilde{T}_B \end{bmatrix} \left(\begin{bmatrix} C_1 X_2^- \\ C_2 X_2^+ \end{bmatrix} \{W_i\} + \begin{Bmatrix} f_p^- \\ f_p^+ \end{Bmatrix} \right) \qquad \text{(B.15)}$$

or

$$f_G = C_2 X_4 W_i + f_{pG} \qquad \text{(B.16)}$$

where $\qquad C_1 = \lceil \sin \alpha, \ \sin \alpha, \ \sin \alpha, \ \cos \alpha \rfloor \qquad$ (B.17)

$$C_2 = \begin{bmatrix} C_1 & 0 \\ 0 & C_1 \end{bmatrix} \qquad \text{(B.18)}$$

Offset transformation effects are included in the displacement and force vectors d_p and f_p, respectively, corresponding to the particular solution functions. d_{pG} and f_{pG} are the corresponding vectors after transformation to global axes. The matrices $C_1 X_1$ and $C_2 X_2$ in conjunction with the vector W_i give the displacements and forces, respectively, corresponding to the complementary solution functions. These matrices include offset effects. The matrices X_3 and X_4 are self-evident and result from transformation to global axes.

In the above equations all quantities except the vector W_i are explicitly known. The matrix C_2 represents the axial (x) distribution of the displacements and forces. Since the Fourier harmonic m, is identical in all elements making up the structure, it is possible to separate out C_2 and drop it from further consideration.

Substituting for W_i from equation (B.14) in equation (B.16), the force-displacement relation for the laminated curved plate-strip element is written as:

$$\left\{\begin{matrix} f_G^- \\ f_G^+ \end{matrix}\right\} = \left[s \right] \left\{\begin{matrix} d_G^- \\ d_G^+ \end{matrix}\right\} - \left\{\begin{matrix} f_r^- \\ f_r^+ \end{matrix}\right\} \tag{B.19}$$

where

$$[s] = \begin{bmatrix} s_{11} & s_{12} \\ & \\ s_{21} & s_{22} \end{bmatrix} = x_4 \cdot x_3^{-1} \tag{B.20}$$

$$s_{21} = s_{12}^T$$

$$\left\{\begin{matrix} f_r^- \\ f_r^+ \end{matrix}\right\} = [s] \left\{\begin{matrix} d_{pG}^- \\ d_{pG}^+ \end{matrix}\right\} - \left\{\begin{matrix} f_{pG}^- \\ f_{pG}^+ \end{matrix}\right\} \tag{B.21}$$

All quantities in equations (B.19) except the displacement vector d_G are explicitly known. The symmetric matrix $[s]$ is analogous to the stiffness matrix of the plate-strip element derived in Ref. 7. Any arbitrary boundary conditions along the external longitudinal (x) side (not connected to other elements) of a plate-strip element are treated in the manner of Ref. 7. Thus, spring constants k_w, k_θ, k_v and k_u with

36

reference to local axes x, y and z, specify the elastic
restraints to freedoms corresponding to the displacements
w, θ, v and u, respectively. A diagonal matrix k_o is defined
as:

$$k_o = \ulcorner k_w, \ k_\theta, \ k_v, \ k_u \lrcorner$$

(B.22)

"Reduced" force-displacement equations may be derived from
equation (B.19) by adopting the method of Ref. 7, when one
side of the plate-strip element is elastically restrained as
above. When the side B $(y = +\frac{b}{2})$ is elastically restrained
the resulting equation is:

$$f_G^- = s_A d_G^- - f_A$$

(B.23)

where

$$s_A = s_{11} - s_{12} \left(s_{22} + k_G^+ \right)^{-1} s_{21}$$

(B.24)

$$k_G^+ = \widetilde{T}_B \cdot k_o \cdot \widetilde{T}_B^{-1}$$

(B.25)

$$f_A = f_{Ao} + f_r^-$$

(B.26)

$$f_{Ao} = - s_{12} \cdot \left(s_{22} + k_G^+ \right)^{-1} \cdot f_r^+$$

(B.27)

Similarly, when the side A $(y = -\frac{b}{2})$ is elastically restrained:

$$f_G^+ = s_B d_G^+ - f_B$$

(B.28)

where

$$s_B = s_{22} - s_{21} \cdot \left(s_{11} + k_G^- \right)^{-1} \cdot s_{12}$$

(B.29)

$$k_G^- = \widetilde{T}_A \cdot k_o \cdot \widetilde{T}_A^{-1}$$

(B.30)

$$f_B = f_{Bo} + f_r^+ \qquad\qquad (B.31)$$

$$f_{Bo} = - s_{21} \cdot \left(s_{22} + k_G^- \right)^{-1} \cdot f_r^- \qquad\qquad (B.32)$$

The symmetric matrices s_A and s_B are analogous to the reduced stiffness matrices of the plate-strip element, derived in Ref. 7.

All equations derived thus far are for the laminated curved plate-strip element. In the limit as the radius $R \rightarrow \infty$, these equations degenerate to those of the laminated flat plate-strip element. For the latter case, some simplifications aiding numerical solution are possible, when the elements of the coupling matrix $[B]$ in equations (A.5) and (A.6) are identically zero. These are discussed in Appendix D of Ref. 7.

B.2 Stiffness of Heated Beam Elements

The temperature change from the ambient conditions in beam elements has the same basic distribution as given by equation (B.1). As for the plate-strip elements, T_x is assumed constant and is again approximated by the truncated Fourier series of equation (B.2).

The displacement functions for a heated beam elements are:

$$w = W_b \sin \alpha$$

$$\theta = \Theta_b \sin \alpha$$

$$v = V_b \sin \alpha \qquad\qquad (B.33)$$

$$u = U_b \cos \alpha$$

where $\alpha = \dfrac{m \pi x}{a}$, m being the Fourier harmonic number.

The above functions are chosen to satisfy the simply supported boundary conditions at the ends $x = 0$ and $x = a$. These displacement functions are substituted in the beam element

equations (A.49) to (A.52). For thermal stress analysis all terms in $\bar{P}_b$ and $\bar{\sigma}$ are omitted since there are no external loads. This results in:

$$f_b = X_5 \, d_b + \bar{f_b} \qquad\qquad\text{(B.34)}$$

The vectors f_t and d_b are defined in equations (A.59) and (A.60), respectively. The elements of the matrix X_5 may be readily derived from equations (A.49) to (A.52). The force vector $\bar{f_b}$ is defined as:

$$\bar{f_b} = \left[\frac{d^2 M_{yT}}{dx^2}, \ 0, \ \frac{d^2 M_{zT}}{dx^2}, \ \frac{dP_T}{dx} \right]^T \qquad\qquad\text{(B.35)}$$

and represents the thermal effects in the heated beam element. The elements of this vector are calculated for each Fourier harmonic, m, using equations (A.53) to (A.55). As for the plate-strip elements, for each value of m it is possible to separate out and drop from further consideration, the axial distributions of the forces and displacements in equation (B.34). Performing the transformation to global axes indicated in equations (A.57) and (A.58), the force-displacement equation for the heated beam element is written as:

$$f_{bG} = s_b \, d_{bG} + \bar{f_{bG}} \qquad\qquad\text{(B.36)}$$

where

$$s_b = T_b \cdot X_5 \cdot T_b^{-1} \qquad\qquad\text{(B.37)}$$

$$\bar{f_{bG}} = T_b \bar{f_b}$$

$$\text{(B.38)}$$

The symmetric matrix s_b is analogous to the beam element stiffness matrix derived in Ref. 7.

39

B.3 Thermal Stress Analysis Formulation

The equations developed thus far are now applied in determining the thermal stresses for an arbitrary structure of uniform cross section shown in Figure 22. Sub-sections B.1 and B.2 give the equations, for individual heated elements relating inter-element boundary global displacement vectors to corresponding force vectors for a chosen Fourier harmonic, m. These are:

(i) "reduced" equations (B.23) and (B.28) for plate-strip elements with specified boundary conditions along one external longitudinal (x) side

(ii) equation (B.19) for any other plate-strip elements

(iii) equation (B.36) for beam elements.

The above equations are given in matrix form. These equations are appropriately merged to satisfy inter-element compatibility and equilibrium in a manner identical to that in the direct stiffness method of finite element analysis. For each Fourier harmonic, m, the resulting equations may be written as:

$$S \, D = F \tag{B.39}$$

The symmetric stiffness matrix S is formed by appropriately merging the element stiffnesses, s_A, s_B and s_b. Since there are no external mechanical loads, the vector F represents thermal effects and is formed from the vectors f_r, f_A, f_B and f_b. D is the yet unknown vector of inter-element boundary displacements corresponding to a particular m-value and is referenced to global axes. Equation (B.39) is solved for these displacements using the symmetric Gaussian elimination algorithm. The resulting d_G^- and d_G^+ vectors for each plate-strip element are substituted in equation (B.13) enabling the evaluation of the corresponding W_i and hence the complementary solution functions of equation (B.6). This, together with the already known particular solution functions of equation (B.7), defines the complete thermal displacement field for a specific value of the Fourier harmonic, m. The corresponding thermal strains in individual plate-strip elements are calculated from equations (A.4). The thermal stresses in beam elements are easily calculated from equations (A.49) to (A.52). The thermal strains and the thermal stresses evaluated for each harmonic, m, are superposed to yield the resultant thermal strains and thermal stresses caused in the structure by the specified thermal field. The decreasing differences between successive resultant stresses, as the number of harmonics retained is increased, indicates that convergence is achieved.

APPENDIX C

BUCKLING ANALYSIS

In certain aerospace structural components like wing panels of high-speed aircraft, thermal stresses vary mainly in the chordwise and thickness directions while remaining nearly constant in the axial direction. Analogous situations exist in some shell type structures, Ref. 24, where the thermal stresses mainly vary in the circumferential and thickness directions. A linear buckling analysis of such heated structures of arbitrary uniform cross section is developed here. The structure is idealized as discussed in Appendix A. All prebuckling deformations are ignored. For buckling of these heated structures under mechanical loads, the inplane normal thermal stresses in plate-strip elements and the axial thermal load in beam elements are treated as preloads on the structure. The latter is kept constant while the former is increased until buckling occurs in some part of the structure. The thermal stresses for a given thermal gradient is directly proportional to the thermal level. Thus a buckling temperature for the structure under given thermal gradients may be determined by proportionately increasing the thermal stresses (for the given thermal gradients and for a chosen thermal level), until buckling occurs in some part of the structure.

The mechanical loading is basically axial compression. However, as in Ref. 7, selected plate-strip elements may have inplane biaxial mechanical loads. A typical example of the latter type of structure is heated stiffened panels under biaxial mechanical loads. In such panels it is reasonable to assume that the inplane mechanical loading transverse to the stiffener axis is carried entirely by the plate-strip elements in the plane of the skin.

The buckling analysis of Ref. 7 is for structures where the loading within each plate-strip element is uniform. The method is versatile in that no assumptions are made regarding the buckling mode shape except that the half-wave length $(\frac{a}{m})$ of buckling is the same in all elements. Transversely, the structure is free to take the buckle shape corresponding to minimum energy conditions consistent with the constraints along any external longitudinal (x) side of plate-strip elements. The nature of buckling is determined from the plot of buckling mode shape resulting from the eigenvector solution.

The method of Ref. 7 is extended here to allow for the variation of the preloads (thermal stresses) in the transverse direction of each plate-strip element. Because of these

variations, the governing differential equations for each plate-strip element have variable coefficients. Using the method of Ref. 9, each such element is sub-divided and the variable coefficient differential equations are reduced to corresponding sets of equivalent constant-coefficient differential equations, one for each sub-division.

Based on these reduced equations, a stiffness matrix for plate-strip elements relating the buckling displacement vectors along the inter-element boundaries to the corresponding forces is derived. For beam elements, the stiffness matrix derived in Ref. 7 is used. These element stiffness matrices are appropriately merged to yield the stiffness matrix of the total structure. The elements of this matrix are transcendental functions of the load level in each element and the longitudinal

(x) half-wavelength $(\frac{a}{m})$ of buckling. For each value of m,

the buckling load is iteratively evaluated from the resulting non-linear eigenvalue problem in the manner of Ref. 7. The minimum of such buckling loads for all possible m-values is then the critical load of the structure. The corresponding eigenvector solution yields the mode shape.

C.1 Stiffness of Plate-Strip Elements with Transversely Varying Preloads

Figure 27 shows the mid-plane (chosen here as the reference plane) of a curved plate-strip element. x, y and z are the local axes. The basic equations (A.15) to (A.17) for such elements include thermal effects. The terms with the additional subscript T are the resulting thermal terms. For the buckling analysis, these additional terms are to be dropped since the thermal stresses are treated as preloads. Subsequent references to these equations implicitly assume that these terms are dropped. The resulting equations are identical to those of Ref. 7. These equations are based on uniform inplane normal external loads of $\bar{N}_{11}$ and $\bar{N}_{22}$. When

the loads vary in the transverse (y) direction, it is easy to see that the resulting differential equations will have variable coefficients. This difficulty is overcome here by using the method of Ref. 9 in the manner outlined below.

The inplane normal loads on the element are given by the stress resultants $\bar{N}_{11}$ (y) in the x direction and $\bar{N}_{22}$ (y) in

the y direction, both varying with y only. These are written as:

$$\bar{N}_{11}(y) = \bar{N}_{1p}(y) + \bar{N}_{1m} \tag{C.1}$$

$$\bar{N}_{22}(y) = \bar{N}_{2p}(y) + \bar{N}_{2m} \tag{C.2}$$

$\bar{N}_{1p}$ (y) and $\bar{N}_{2p}$ (y) are the preloads (thermal stresses) varying with y only. $\bar{N}_{1m}$ and $\bar{N}_{2m}$ are the additional uniform mechanical loads.

The plate-strip element is sub-divided into a series of equal sub-elements (1), (2), ...(g) as shown in Figure 27. As the number of sub-elements in increased, (thus decreasing their size) the amplitude of the variable coefficients in the differential equations decreases. In the limiting case, when the sub-elements are infinitesimally small, these variable coefficients approach a fixed value. The original differential equations with variable coefficients may then be approximated by sets of constant coefficient equations, identical to equations (A.15) to (A.17), one set for each sub-element. A relatively small number of sub-elements will usually suffice to yield accurate results, as shown in Ref. 9. The constant coefficient equations for each sub-element are satisfied in an exact manner. Continuity is achieved between sub-element regions from compatibility and equilibrium considerations.

Figure 7.1 also shows the sub-element (j) of width $\bar{b}$ and the local axes $\bar{x}$, $\bar{y}$ and $\bar{z}$. The assumed buckling displacement function for each sub-element is:

$$\bar{w} = \sum_{i=1}^{8} \bar{W}_i \, e^{\bar{\beta}_i} \sin \alpha$$

$$\bar{v} = \sum_{i=1}^{8} \bar{V}_i \, e^{\bar{\beta}_i} \sin \alpha \tag{C.3}$$

$$\bar{u} = \sum_{i=1}^{8} U_i \, e^{\bar{\beta}_i} \cos \alpha$$

where:

$$\bar{\beta}_i = \frac{\bar{p}_i \, \pi y}{a} \qquad \text{and} \quad \alpha = \frac{m\pi x}{a}$$

$\bar{p}_i$ (i = 1, 2, ...8) are the roots of the characteristic

equation discussed below. The longitudinal (x) half-wave
number, m, is by necessity the same in all elements of
the structure. The above functions are chosen to satisfy
ab initio the simply supported boundary conditions along
the edges $x = 0$ and $x = a$. At any level of external loading
an average value of $\bar{N}_{11}$ (j) and $\bar{N}_{22}$ (j) in sub-element (j)

may be calculated from equations (C.1) and (C.2). In practice,
for each sub-element, the values calculated along $\bar{y} = 0$
would suffice. These external load values, together with
buckling displacement functions, are substituted in equations
(A.15) to (A.17) to yield a characteristic polynominal in $\bar{p}_i$,
identical in form to equation (B.10). Using these $\bar{P}_i$
values, the buckling displacements and the corresponding

forces along the boundaries $\bar{y} = -\dfrac{\bar{b}}{2}$ and $\bar{y} = +\dfrac{\bar{b}}{2}$ of each

sub-element are evaluated as in Ref. 7. Thus, for sub-
element (j):

$$\left\{ \begin{array}{c} \bar{d}^{-} \\ \\ \bar{d}^{+} \end{array} \right\}_{(j)} = \left[\begin{array}{c} C_1 \bar{X}_1 \\ \\ C_1 \bar{X}^{+} \end{array} \right]_{(j)} \cdot \left\{ \bar{w}_i \right\}_{(j)} \tag{C.4}$$

$$\left\{ \begin{array}{c} \bar{f}^{-} \\ \\ \bar{f}^{+} \end{array} \right\}_{(j)} = \left[\begin{array}{c} C_1 \bar{X}_2 \\ \\ C_1 \bar{X}_2^{+} \end{array} \right]_{(j)} \cdot \left\{ \bar{w}_i \right\}_{(j)} \tag{C.5}$$

These equations are with respect to the local coordinates.
The elements of each sub-vector $\{d\}$ and $\{f\}$ are readily
identified from equations (A.24) to (A.27). The matrices
X and X are analogous to X_1 and X_2 in equations (B.13) and

(B.15). C_1, defining the longitudinal (x) distribution of

the forces and displacements, is given by equation (B.17).
These distributions, being identical in all elements, may be
separated out and omitted from further consideration. The
above equations are used in ensuring continuity between the
sub-elements. This may be achieved by two somewhat similar
methods.

In the first method a symmetric stiffness matrix is
derived for each sub-element from equations (C.4) and (C.5),

as in Ref. 7, relating the forces and displacements. This is written as:

$$\left\{ \begin{array}{c} \bar{f}^{-} \\ \\ \bar{f}^{+} \end{array} \right\}_{(j)} = [\bar{s}]_{(j)} \left\{ \begin{array}{c} \bar{d}^{-} \\ \\ \bar{d}^{+} \end{array} \right\}_{(j)} \tag{C.6}$$

Now, considering sub-elements (1) and (2), the respective sub-element stiffness matrices are appropriately merged and the degrees of freedom along the common boundary are reduced to give:

$$\left\{ \begin{array}{c} \bar{f}^{-}_{(1)} \\ \\ \bar{f}^{+}_{(2)} \end{array} \right\} = [\bar{s}]_{(1-2)} \left\{ \begin{array}{c} \bar{d}^{-}_{(1)} \\ \\ \bar{d}^{+}_{(2)} \end{array} \right\} \tag{C.7}$$

where $[s]_{(1-2)}$ is the symmetric reduced stiffness matrix. By

successively merging the stiffness matrices of adjacent sub-elements and reducing the interior freedoms at each step, the resulting equation becomes:

$$\left\{ \begin{array}{c} \bar{f}^{-}_{(1)} \\ \\ \bar{f}^{+}_{(g)} \end{array} \right\} = [\bar{s}]_{(1-g)} \left\{ \begin{array}{c} \bar{d}^{-}_{(1)} \\ \\ \bar{d}^{+}_{(g)} \end{array} \right\} \tag{C.8}$$

where $[s]_{(1-g)}$ is the required symmetric stiffness matrix of

the curved plate-strip element, when the external loads are varying in the transverse (y) direction. Instead of successively merging and reducing at each sub-element level as described above, it is possible to merge the stiffness of all sub-elements at one time and perform one large reduction of all interior freedomes.

In the second method, continuity conditions imposed through equations (C.4) and (C.5) are used to relate $\bar{w}_i$'s of successive

sub-elements to $\{\bar{w}_i\}_{(1)}$. Thus for sub-element (2):

$$\left\{ \bar{w}_i \right\}_{(2)} = \left[\begin{array}{c} \bar{x}^{-}_{1} \\ \\ -\bar{x}^{-}_{2} \end{array} \right]^{-1}_{(2)} \left[\begin{array}{c} \bar{x}^{+}_{1} \\ \\ \bar{x}^{+}_{2} \end{array} \right]_{(1)} \left\{ \bar{w}_i \right\}_{(1)} \tag{C.9}$$

or

$$\left\{ \bar{w}_i \right\}_{(2)} = [\bar{C}]_{(2)} \left\{ \bar{w}_i \right\}_{(1)}$$

Similarly,

$$
\left\{\bar{w}_i\right\}_{(3)} = \begin{bmatrix} \bar{x}_1 \\ \\ -\bar{x}_2 \end{bmatrix}_{(3)}^{-1} \begin{bmatrix} \bar{x}_1^+ \\ \\ \bar{x}_2^+ \end{bmatrix}_{(2)} \left\{\bar{w}_i\right\}_{(2)}
\tag{C.10}
$$

The matrices involved in the above equations are unsymmetric. Substituting for $\left\{\bar{w}_i\right\}_{(2)}$ from equation (C.9):

$$
\left\{\bar{w}_i\right\}_{(3)} = [\bar{C}]_{(3)} \left\{\bar{w}_i\right\}_{(1)}
\tag{C.11}
$$

The matrix $[\bar{C}]_{(3)}$ is self-evident. Continuing this procedure to the last sub-element (g) yields:

$$
\left\{\bar{w}_i\right\}_{(g)} = [\bar{C}]_{(g)} \left\{\bar{w}_i\right\}_{(1)}
\tag{C.12}
$$

Also, for the boundary $\bar{y} = -\dfrac{b}{2}$ of sub-element (1):

$$
\left\{\begin{array}{c} \bar{d}^- \\ \\ \bar{f}^- \end{array}\right\}_{(1)} = \begin{bmatrix} \bar{x}_1^- \\ \\ \bar{x}_2^- \end{bmatrix}_{(1)} \left\{\bar{w}_i\right\}_{(1)}
\tag{C.13}
$$

Similarly for the boundary $\bar{y} = +\dfrac{b}{2}$ of sub-element (g):

$$
\left\{\begin{array}{c} \bar{d}^+ \\ \\ \bar{f}^+ \end{array}\right\}_{(g)} = \begin{bmatrix} \bar{x}_1^+ \\ \\ \bar{x}_2^+ \end{bmatrix}_{(g)} \left\{\bar{w}_i\right\}_{(g)}
\tag{C.14}
$$

or

$$
\left\{\begin{array}{c} \bar{d}^+ \\ \\ \bar{f}^+ \end{array}\right\}_{(g)} = \begin{bmatrix} \bar{x}_1^+ \\ \\ \bar{x}_2^+ \end{bmatrix}_{(g)} [\bar{C}]_{(g)} \left\{\bar{w}_i\right\}_{(1)}
\tag{C.15}
$$

After partititioning suitably, the stiffness matrix of the curved plate-strip element under transversely (y) varying external loads is readily derived from equations (C.13) and (C.15). The result is identical to equation (C.8).

In the first method the inversion process concerns symmetric matrices whereas in the second method unsymmetric matrices are involved. The stiffness matrix derived by either method is based on equations (C.4) and (C.5) which are in local coordinates. A coordinate transformation on equation (C.8) yields the global force-displacement relationship for a curved plate-strip element as:

$$
\begin{Bmatrix} f_G^- \\ \cdot \\ f_G^+ \end{Bmatrix} = \begin{bmatrix} \widetilde{T}_A & 0 \\ & \\ 0 & \widetilde{T}_B \end{bmatrix} [\bar{s}] \begin{Bmatrix} d_g^- \\ \\ d_g^+ \end{Bmatrix}
$$

$$
= [s] \begin{Bmatrix} d_G^- \\ \\ d_G^+ \end{Bmatrix}
$$

(C.16)

The sub-vectors d_G and f_G are defined in equations (4.44) and (A.46), respectively.

The buckling analysis allows arbitrary elastic restraints (specified by spring constants) along any external longitudinal (x) side of the curved plate-strip elements. For such elements reduced stiffness matrices are easily derived as in Ref. 7. Thus, when the side $y = +\dfrac{b}{2}$ of the element is elastically restrained:

$$
f_G^- = s_A d_G^-
$$

(C.17)

and when the side $y = \dfrac{b}{2}$ is elastically restrained:

$$
f_G^+ = s_B d_G^+
$$

(C.18)

s_A and s_B are the reduced stiffnesses.

The elements of the stiffness matrices in equations (C.16) to (C.18) are transcendental functions of the load level in the structure and the longitudinal (x) half-wave number, m.

The analysis presented in this section for curved plate-strip elements degenerates to that of a flat plate-strip element in the limit as the radius $R \to \infty$. In this case certain simplifications aiding numerical solution are possible and are discussed in Appendix D of Ref. 7.

C.2   Stiffness of Beam Elements

The axial thermal loads are treated as preloads. The external mechanical load is superposed on this. The stiffness of the beam element subjected to the resultant axial load is easily derived as in Ref. 7 and results in

$$f_{bG} = s_b \, d_{bG}$$
(C.19)

The vectors f_{bG} and d_{bG} are defined in equation (A.53) and (A.54).

C.3   Buckling Formulation

The equations developed thus far are applied in formulating the buckling criterion for the arbitrary structure of uniform cross section shown in Figure 22.   The method being the same as in Ref. 7, only an outline is given below.

The structure is idealized as described in Appendix A. By necessity the number of longitudinal (x) half-waves, m, is identical in all elements of the structure. As indicated earlier, the analysis assumes that the thermal stresses do not vary in the longitudinal direction. However, if such variations do exist and are not too severe, a buckling solution of reasonable accuracy may be obtained using thermal stresses averaged in the longitudinal direction. Alternatively, the peak stress in the longitudinal direction may be used as illustrated for the buckling of a cylinder heated on an axial strip, in Ref. 5.

In buckling under combined thermal gradients and mechanical loads, the thermal stresses are treated as preloads which remain constant. Thus different levels of loading are defined by changes in mechanical loading. The distribution of mechanical loading among the various elements in the structure, corresponding to any level of loading, is obtained from strain compatibility considerations, as in Ref. 7. Superposing these element loadings on the preloads (thermal stresses), the stiffness matrices are evaluated for various elements in the structure, for a chosen value of m. These are merged to yield the stiffness matrix of the total structure. This procedure is analogous to that described in Appendix B. The resulting equation is:

$$S \cdot D = 0$$
(C.20)

where   S   is the merged stiffness matrix and   D   is the vector of the inter-element boundary displacements. For a non-trivial solution, the buckling criterion is written in the determinantal form:

$$|S| = 0$$
(C.21)

48

The elements of the symmetric matrix S are trans-cendental functions of the load level in the structure and the longitudinal (x) half-wavelength of buckling $(\frac{a}{m})$. Thus the above equation does not correspond to standard algebraic eigenvalue problems. For the chosen longitudinal half-wave number, m, the lowest level of external loading at which equation (C.21) is satisfied is the buckling load of the structure. This is determined iteratively using the algorithm described in Ref. 7. An upper bound to the buckling load of the structure, determined from the buckling load of individual elements when the inter-element boundaries are completely restrained, is crucial to the success of the algorithm. A method to evaluate the buckling loads of these "restrained" elements subjected to transversely (y) varying preloads and uniform mechanical loads, is discussed in sub-section C.4.

The lowest of all buckling loads of the structure for a series of m-values is then the critical load. The corres-ponding vector D in equation (C.20) giving the inter-element boundary displacements, is obtained by Wielandt's method of inverse iteration, Ref. 25.

In order to calculate the distribution of the buckling displacements across the width of each plate-strip element, it is necessary to know the $\overline{W}_i$ coefficients in equation (C.3), for each sub-element. These are calculated from the known element boundary displacements, using equations (C.4) and (C.8) or equations (C.4) and (C.12).

For beam elements the eigenvector solution directly gives the global buckling displacements of the shear center.

A plot of w and v displacements of each element across the cross section of the structure identifies the buckled elements and indicates whether buckling is local or general. Such plots may be used in achieving efficient design of structures as illustrated in Refs. 14 and 26.

The generality of the buckling analysis presented here is discussed and illustrated in Ref. 7.

C.4 Upper Bound to Buckling Load

The principle of the method is to determine a buckling
load P_r for each element, corresponding to the chosen value

of the longitudinal (x) half-wave number m for the structure,
when the inter-element boundaries are completely restrained.
The smallest of the P_r values is then the upper bound load

to the buckling load of the structure, for the chosen m-value.
Obviously, the beam elements may be ignored from these con-
siderations. Thus, only plate-strip elements with either edges
fully restrained or one edge fully restrained and the other
edge arbitrarily restrained by specified spring constants,
are considered.

In the manner of sub-section C.1, each "restrainted"
plate-strip element is divided into sub-elements as shown in
Figure 27.   The transversely-varying preloads (thermal stresses)
are approximated by uniform values in each sub-element. The
buckling load of each "restrained" element (for a chosen m-value
for the structure) is obtained by formulating the corresponding
buckling problem in the form of equation (C.21). This is
achieved by merging the stiffness of each sub-element and
taking into account the restraints along the longitudinal (x)
sides of the "restrained" element. Since a completely re-
strained side has zero displacements, the corresponding rows
and columns of the merged stiffness matrix are deleted. The
resulting matrix is the buckling determinant from which the
buckling load is evaluated iteratively. An upper bound to the
"restrained" element buckling problem is obtained using the
Galerkin method, as described in Appendix E of Ref. 7.

REFERENCES

1. Boley, Bruno A., Weiner, Jerome H.: Theory of Thermal Stresses, John Wiley & Sons, 1960.

2. Hoff, N. J. (Editor): High Temperature Effects in Aircraft Structures, AGARDograph No. 28, Pergamon Press, 1958.

3. Johns, D. J.: Thermal Stress Analyses, Pergamon Press, 1965.

4. Chang, L. K. and Card, Michael F.: Thermal Buckling Analysis for Stiffened Orthotropic Cylindrical Shells. NASA TN D-6332, April 1971.

5. Bushnell D., Smith S.: Stress and Buckling of Nonuniformly Heated Cylindrical and Conical Shells, AIAA Journal, Vol. 9, No. 12, December 1971, pp. 2314-2321.

6. Hoff, N. J.: Buckling at High Temperature. Jour. of Royal Aeronautical Society, Vol. 61, No. 11, November 1957.

7. Viswanathan, A. V., Tamekuni, M.: Elastic Buckling Analysis for Composite Stiffenened Panels and Other Structures Subjected to Biaxial Inplane Loads. NASA CR 2216, 1973.

8. Viswanathan, A. V., Soong, T. C., Miller, Jr., R. E., Compressive Buckling Analysis and Design of Stiffened Flat Plates with Multilayered Composite Reinforcement. Presented at the National Symposium on Computerized Structural Analysis and Design, George Washington University, Washington, D. C., March 1972.

9. Soong, T. C.: A Subdivisional Method for Linear Systems, Proceedings of the AIAA/ASME 11th Structures, Structural Dynamics and Materials Conference (Denver), AIAA, New York, 1970.

10. Tripp, Leonard L., Tamekuni, M., Viswanathan, A. V.: A Computer Program for Stresses and Buckling of Heated Composite Stiffened Panels and Other Structures" Users Manual for "BUCLASP3" NASA CR 112,228, 1973.

11. Connacher, N., McElroy, M., Hansen, S. D.: SAMECS Structural Analysis System: Users Document. D6-23757-1TN. The Boeing Company, Commercial Airplane Group, Seattle, February 1969.

12. Hoff, N. J.: Buckling of Thin Cylindrical Shell Under Hoop Stresses Varying in Axial Direction. J. of App. Mechanics, September 1957, pp. 405-412.

13. Kalnins, Arturs: Static, Free Vibration and Stability
Analysis of Thin, Elastic Shells of Revolution.
AFFDL-TR-68-144, Air Force Flight Dynamics Laboratory
Wright-Patterson Air Force Base, Ohio, March 1969.

14. Tripp, Leonard L, Tamekuni, M., Viswanathan, A. V.: A
Computer Program for Instability Analysis of Biaxially
Loaded Composite Stiffened Panels and Other Structures:
Users Manual for "BUCLASP2", NASA CR 112,226, 1973.

15. Timoshenko, S. P., Gere, J. M.: Theory of Elastic
Stability, McGraw-Hill, 2nd edition, 1961.

16. Abir, D., Nardo, S. V.: Thermal Buckling of Circular
Cylindrical Shells under Circumferential Temperature
Gradients. J. of Aerospace Sciences, Vol. 26, No. 12,
December 1959, pp. 803-808.

17. Bijlaard, P. P., Gallagher, R. H.: Elastic Instability of
a Cylindrical Shell Under Arbitrary Circumferential
Variation of Axial Stress. J. of Aerospace Sciences,
Vol. 27, No. 11, November 1960, pp. 854-858 and 866.

18. Soong, T. C.: Buckling of Cylindrical Shells with Eccentric
Spiral-Type Stiffeners. AIAA Journal, Vol. 7, No. 1,
January 1969, pp. 65-72.

19. Dong, S. B., Foye, R. L.: Structural Design Guide for
Advanced Composite Applications: Stress and Deformations,
2nd edition, Air Force Materials Laboratory, Wright-Patterson
Air Force Base, Ohio, January 1971.

20. Novozhilov, V. V.: Thin Shell Theory, P. Nordhoff, Ltd.,
Netherlands, 1964.

21. Boley, Bruno A.: Bounds for the Torsional Rigidity of
Heated Beams, AIAA Journal, Vol. 9, No. 3, March 1971,
pp. 524, 525.

22. Hemp, W. S.: Thermo-Elastic Formulae for the Analysis
of Beams, Aircraft Engineering, November 1956, pp. 374-376.

23. Boley, Bruno, A.: On Thermal Stresses in Beams: Some
Limitations of the Elementary Theory. Int. J. of Solids
and Structures, Vol. 8, 1972, pp. 571-579.

24. Anderson, Melvin S.: "Collected Papers on Instability of
Shell Structures - 1962": Thermal Buckling of Cylinders
NASA TN D-1510, December 1962.

25. Wilkinson, J. H.: The Algebraic Eigenvalue Problem,
Clarendon Press, 1965.

26. Viswanathan, A. V., Soong, Tsai-Chen, Miller, Jr., R. E.:
    Buckling Analysis for Structural Sections and Stiffened
    Plates Reinforced with Laminated Composites. Int. J. of
    Solids and Structures, Vol. 8, pp. 347 to 367, 1972.

27. Mechtly, E. A.: The International System of Units -
    Physical Constants and Conversion Factors (Revised).
    NASA SP-7012, 1969.

Material Properties:

Plate: $E_{11} = E_{22} = 10.0 \times 10^6$ lbs/in^2
$\quad G_{12} \quad\quad = 3.85 \times 10^6$ lbs/in^2
$\quad \nu_{12} \quad\quad = 0.3$

Rod: $E_{11} = 10.0 \times 10^6$ lbs/in^2
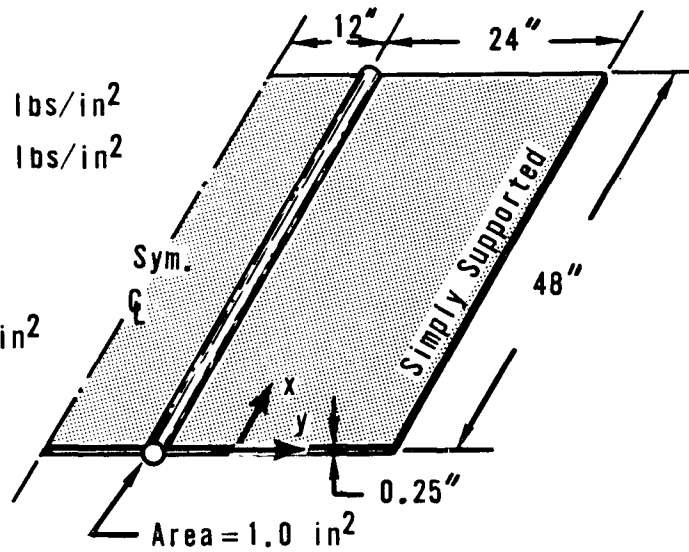
Figure 1.   Isotropic Flat Plate with Two "Rod" Stiffeners
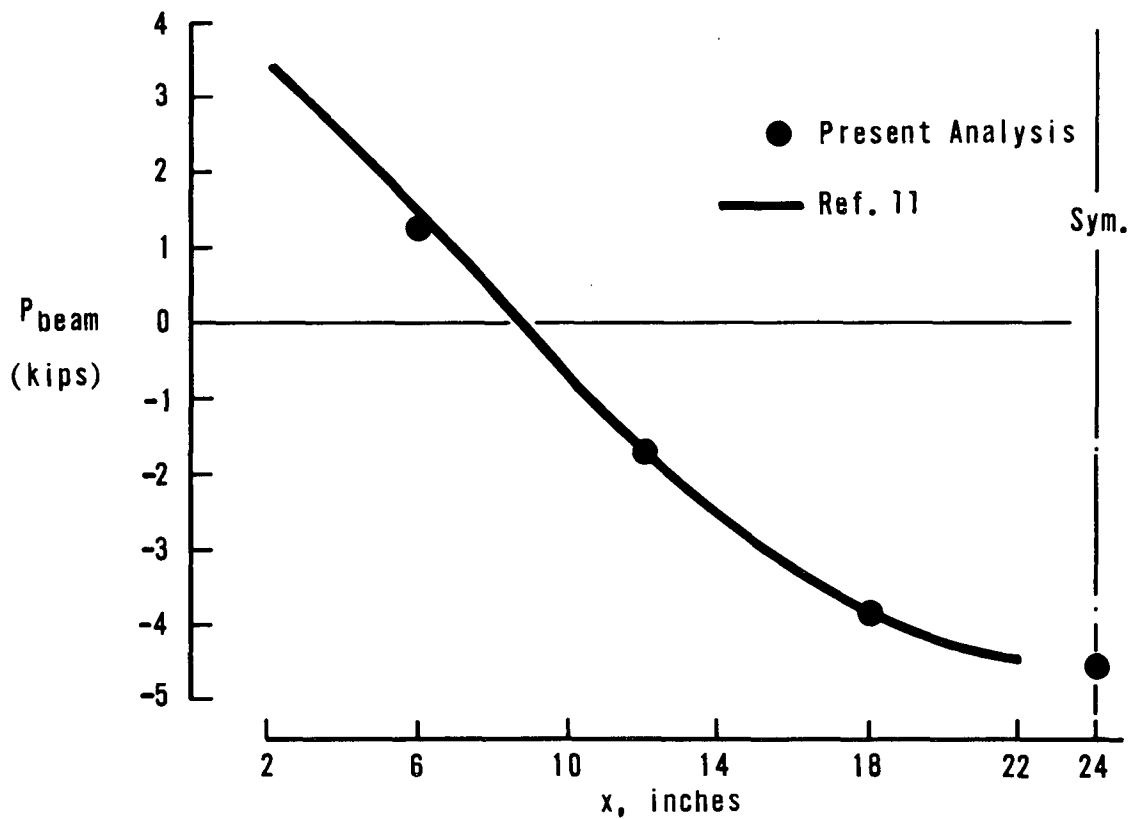
Figure 2.   Thermal Stress in the "Rod"   (1 of 2)
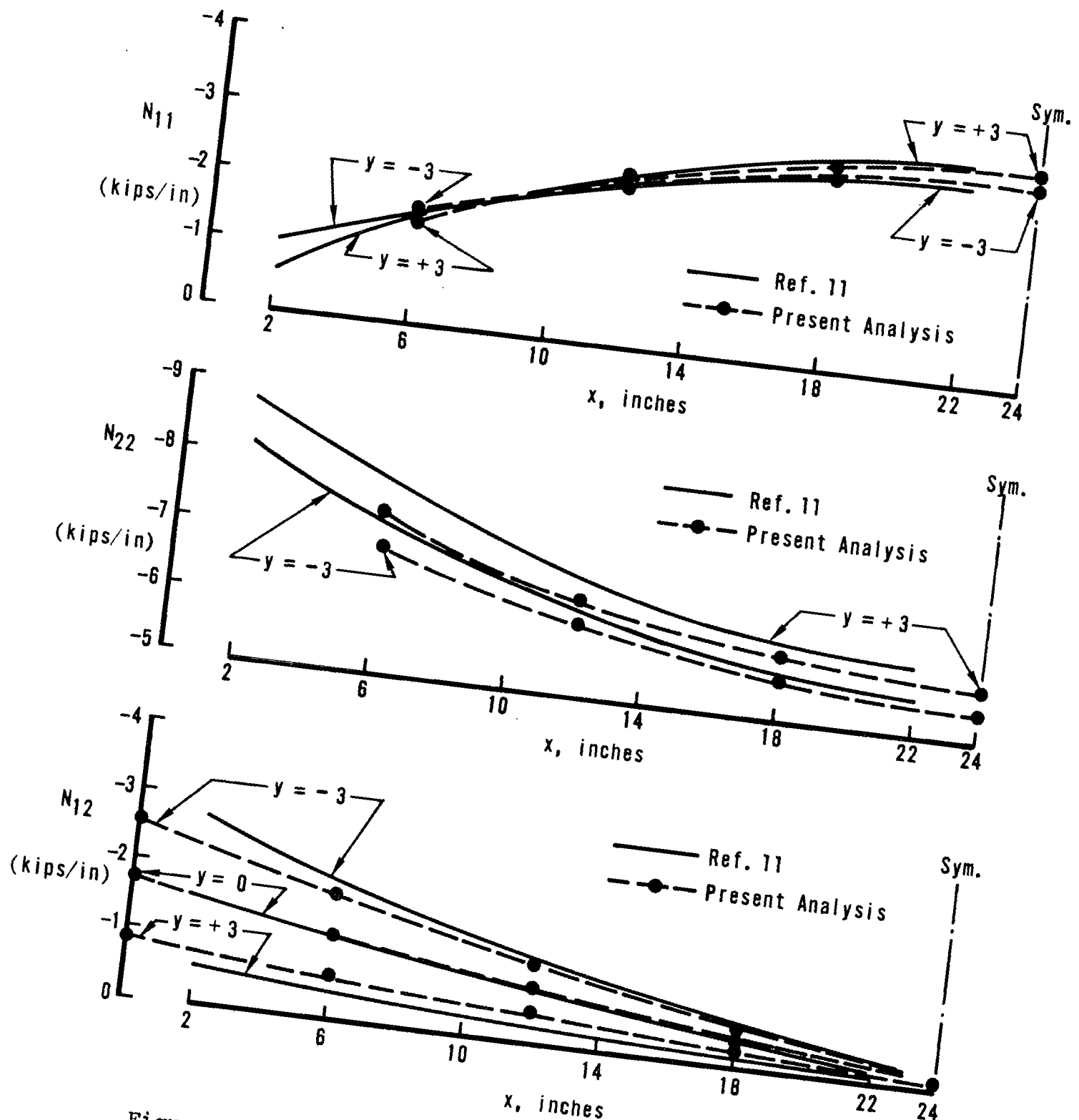
Figure 2. Thermal Stress in Plate (2) (2 of 2)
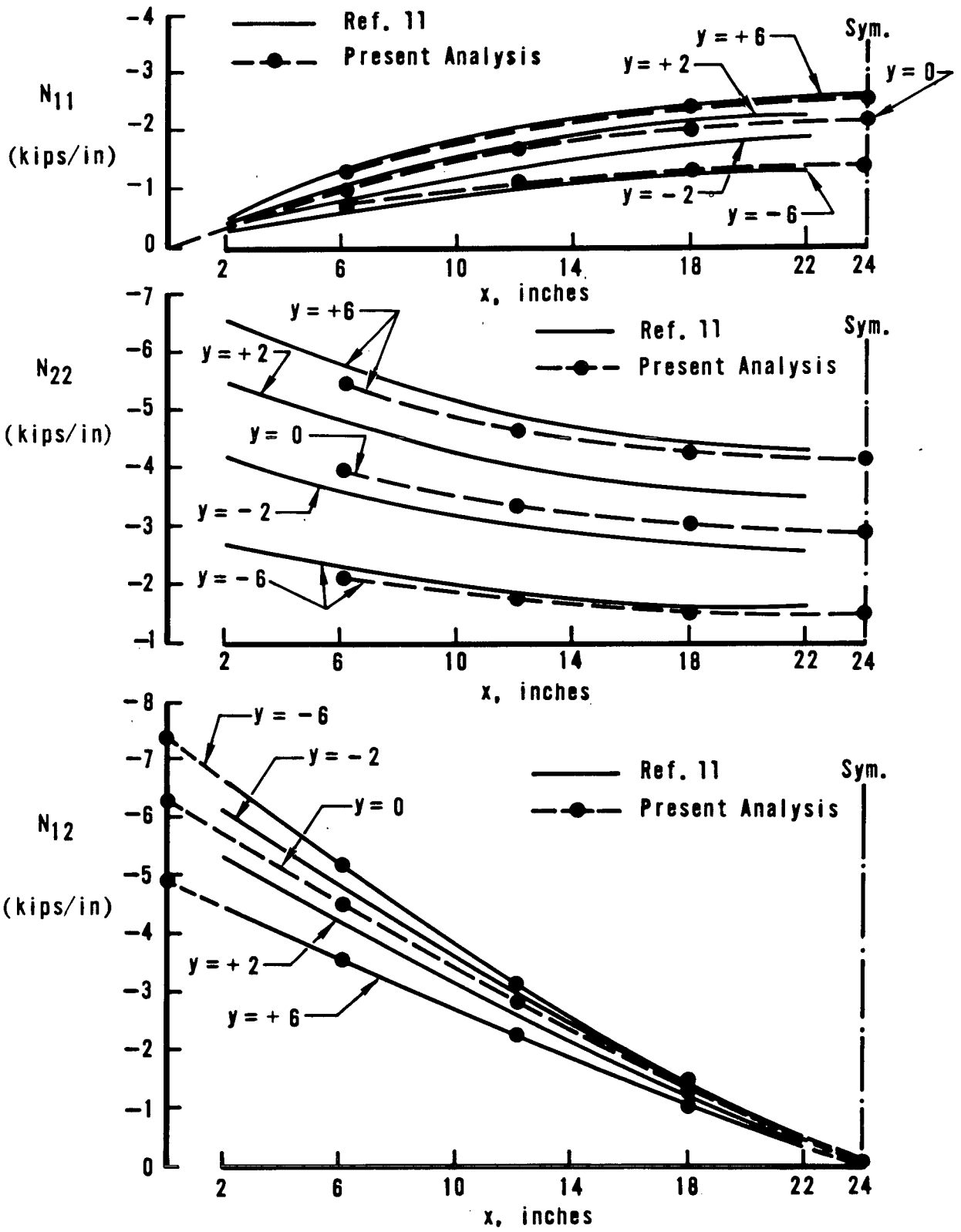
Figure 3. Thermal Stress in Plate (1)

Cylinder	Mid plane Radius, R Inches	t, Inches	Length, a, Inches
A	10.0	0.0331	3.14
B	10.0	0.25	30.0
C	5.18	0.008	48.0

Material Properties

Cylinder	$E_{11} \times 10^{-6}$ lbs/in^2	$E_{22} \times 10^{-6}$ lbs/in^2	$G_{12} \times 10^{-6}$ lbs/in^2	ν_{12}	$\alpha_T \times 10^6$ in/in/^{0}F
A	29.0	29.0	11.15	0.3	7.241
B	10.0	10.0	3.85	0.3	10.0
C	30.0	30.0	11.53	0.3	6.0
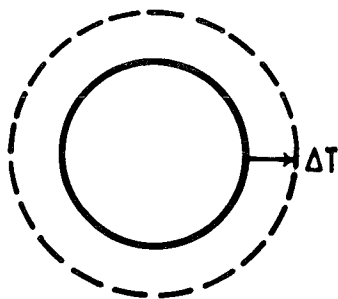
$\Delta T = 600^0 F$
Cylinder A
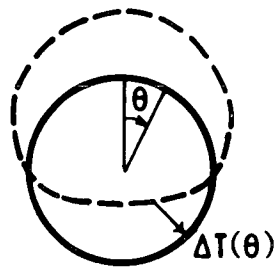
$\Delta T = (100 \cos \theta)^0 F$
Cylinder B
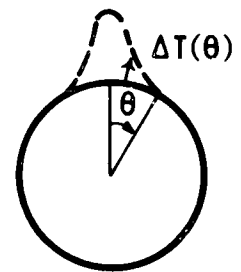
$\Delta T = (\Delta T_0 e^{-50\theta^2})^0 F$
$(\Delta T_0 = 1)$
Cylinder C

Figure 4. Isotropic Cylinders
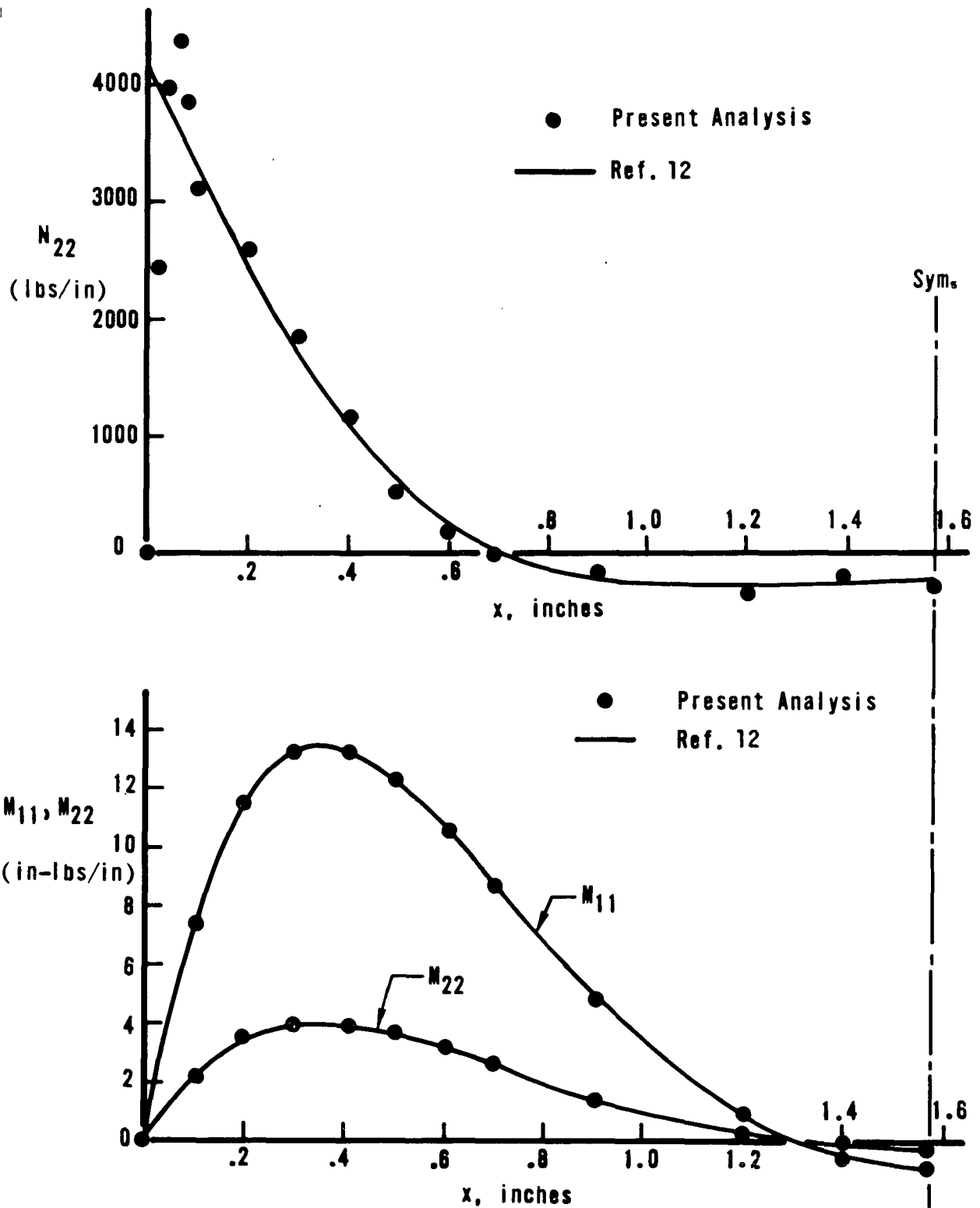
Figure 5. Thermal Stress in Cylinder A
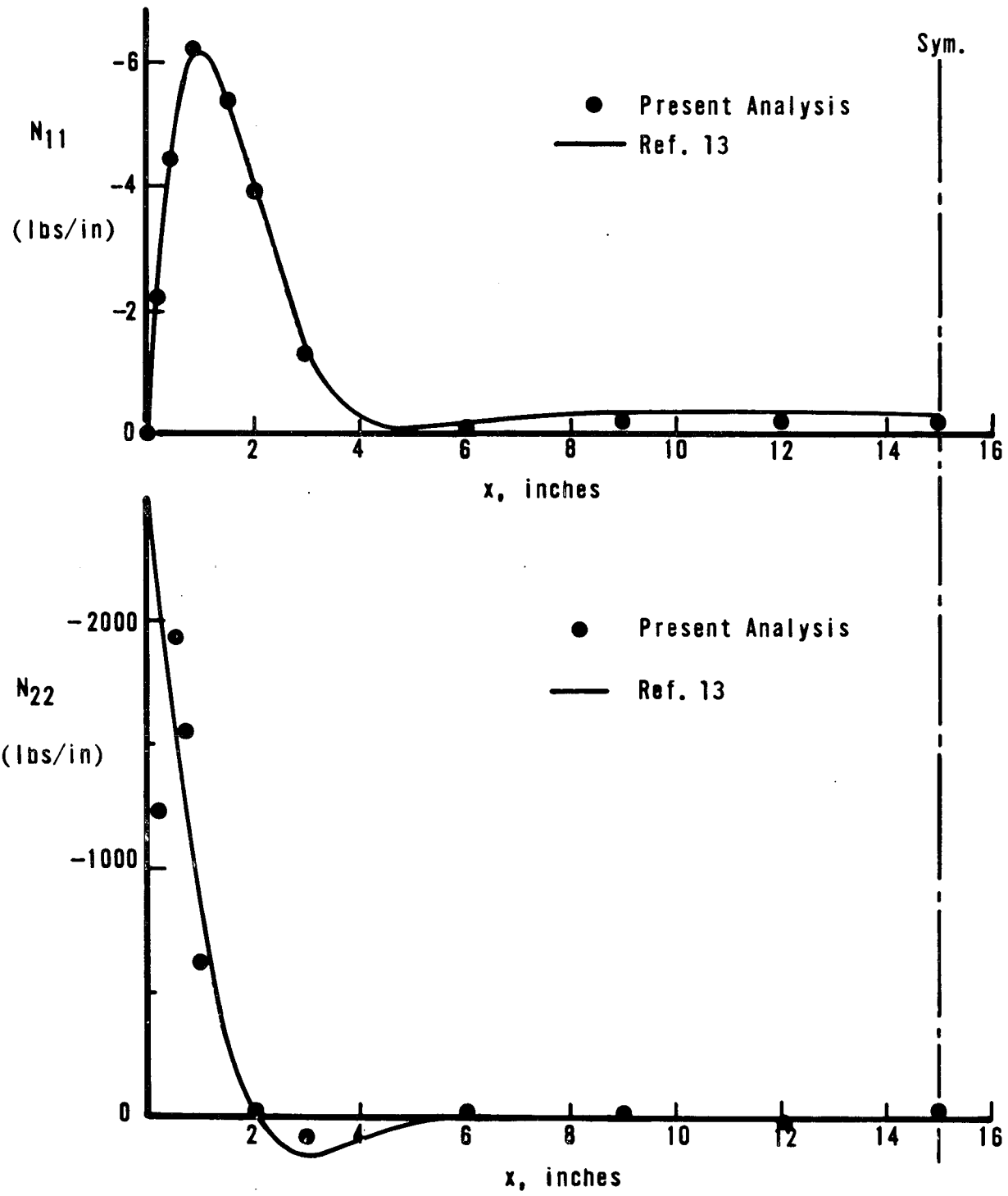
Figure 6. Thermal Stress in Cylinder B (1 of 2)
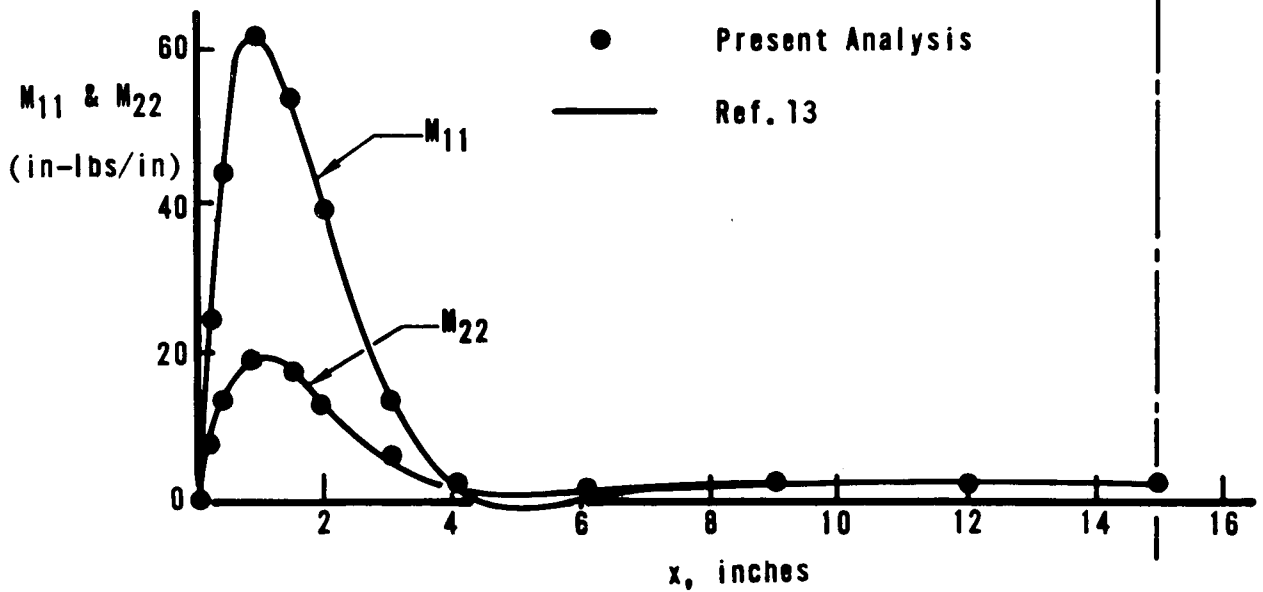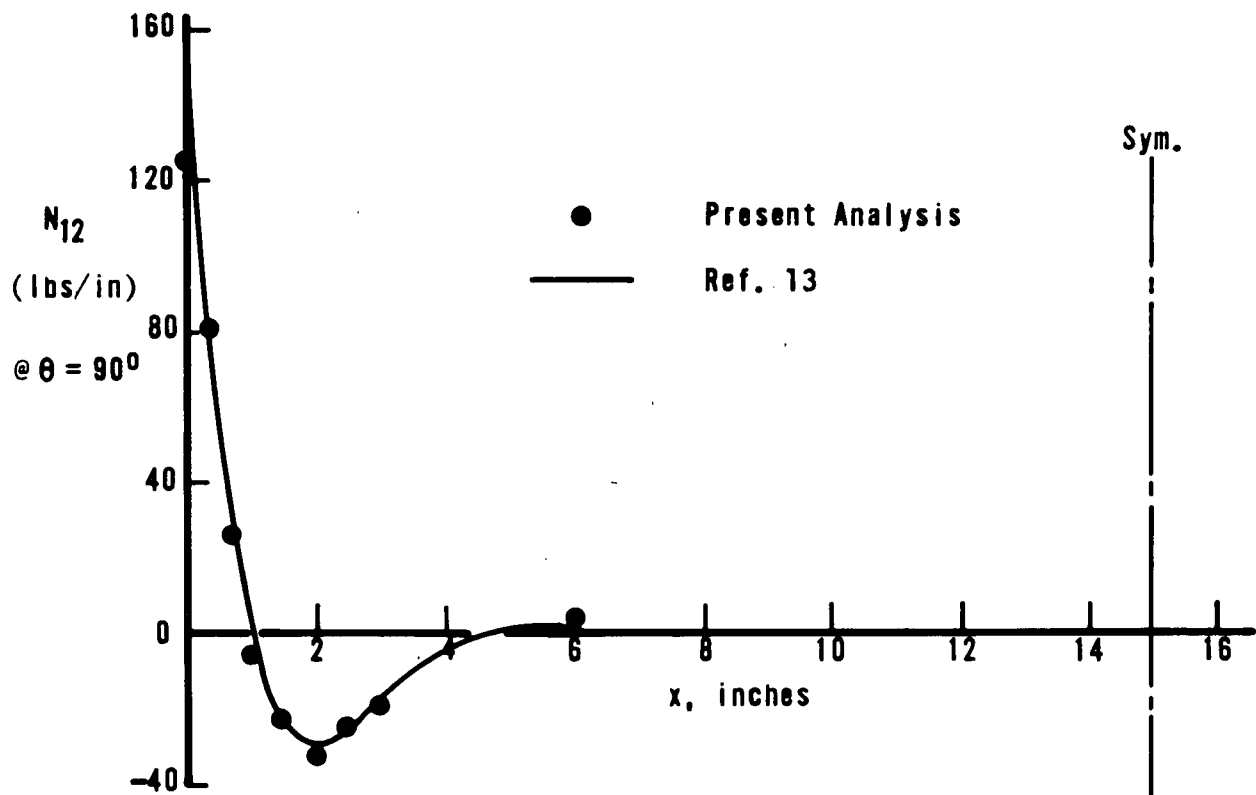
Figure 6. Thermal Stress in Cylinder B (2 of 2)
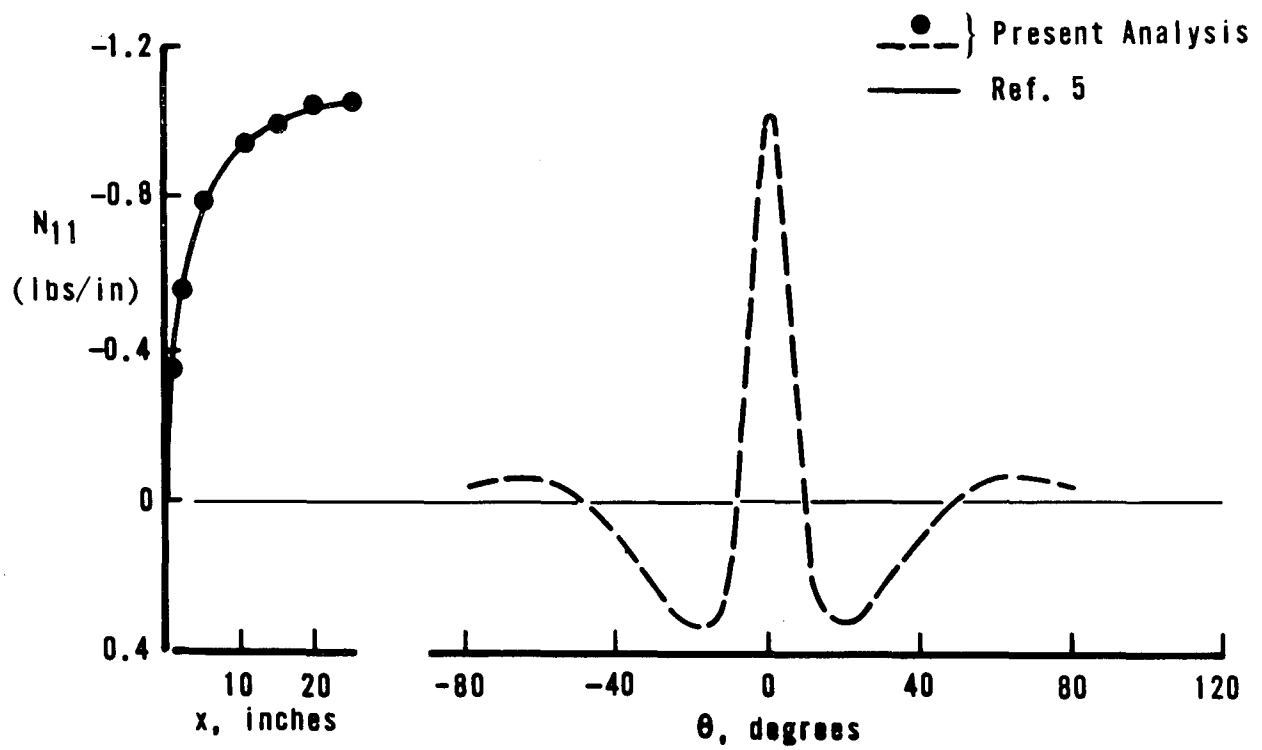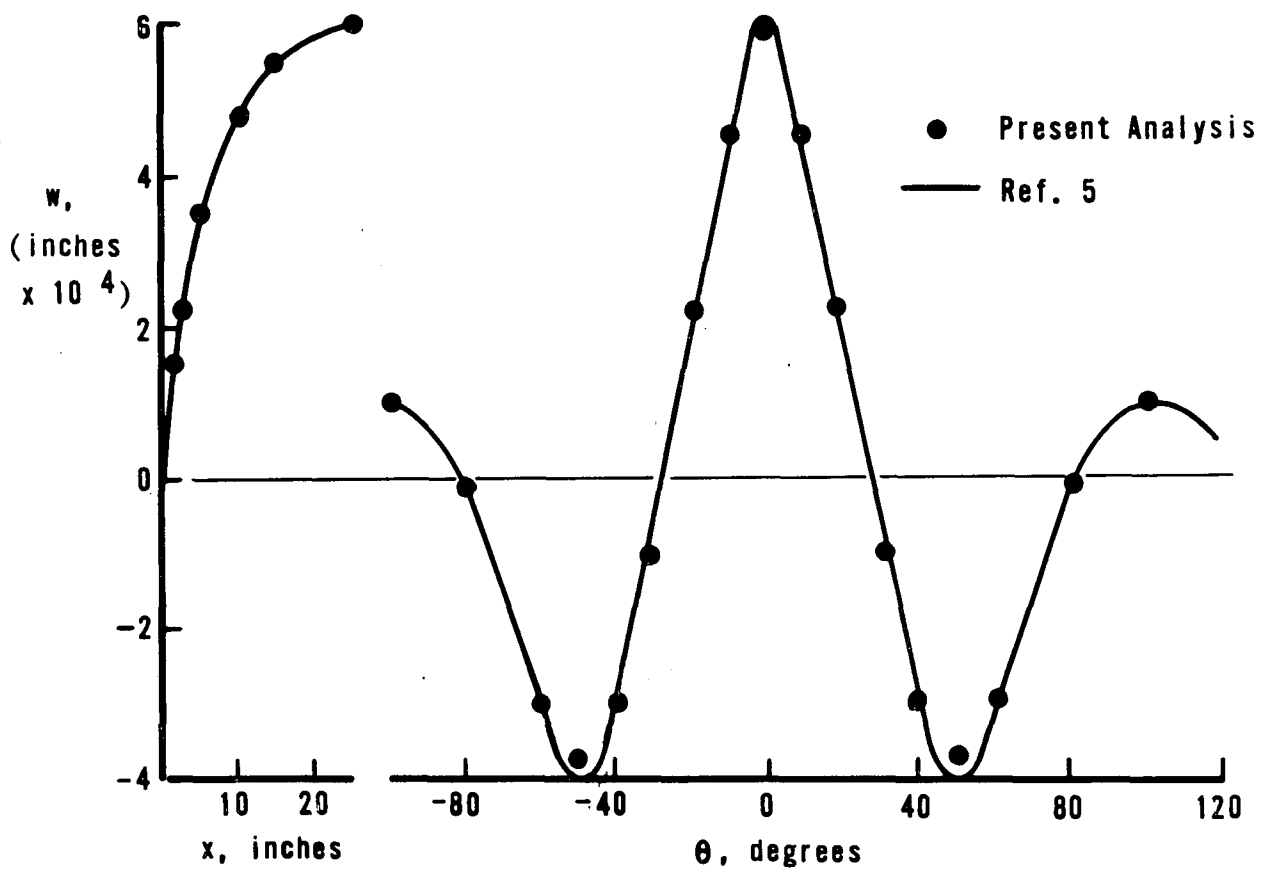
Figure 7. Results for Cylinder C
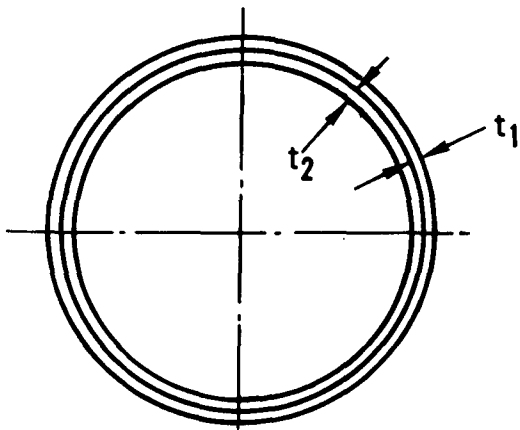
Mid-plane radius = 10.0 inches
Length = 30.0 inches
$t_1 = t_2$ = 0.5 inches
ΔT = 400°F

Material Properties

Shell	$E_{11} \times 10^{-6}$ lbs/in^2	$E_{22} \times 10^{-6}$ lbs/in^2	$G_{12} \times 10^{-6}$ lbs/in^2	ν_{12}	$\alpha_T \times 10^6$ in/in/°F
Inner	15.0	15.0	6.0	0.25	6.0
Outer	10.4	10.4	3.91	0.33	12.7

Figure 8. Laminated Cylinder
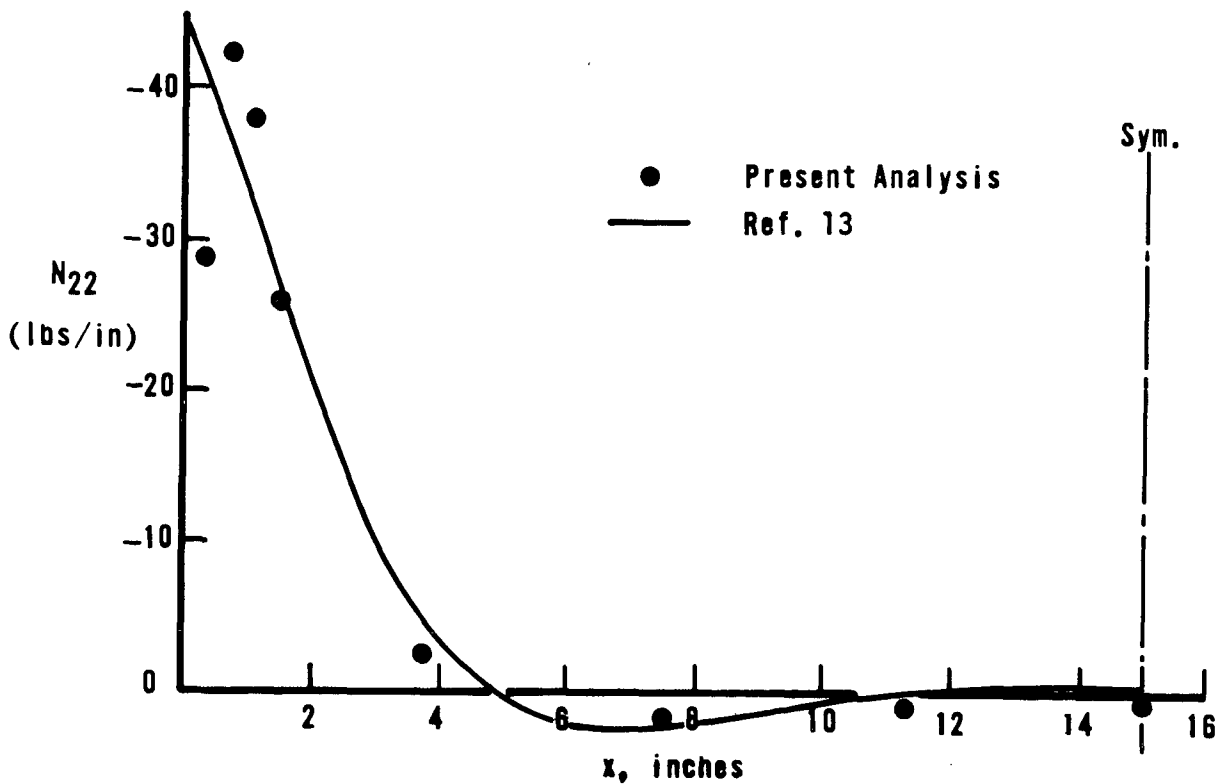
Figure 9. Thermal Stress in Laminated Cylinders (1 of 2)

Figure 9. Thermal Stress in Laminated Cylinders (2 of 2)

Internal Stringers

R = 30″

15″

60″

6.28″

0.22″

1.687″

0.163″
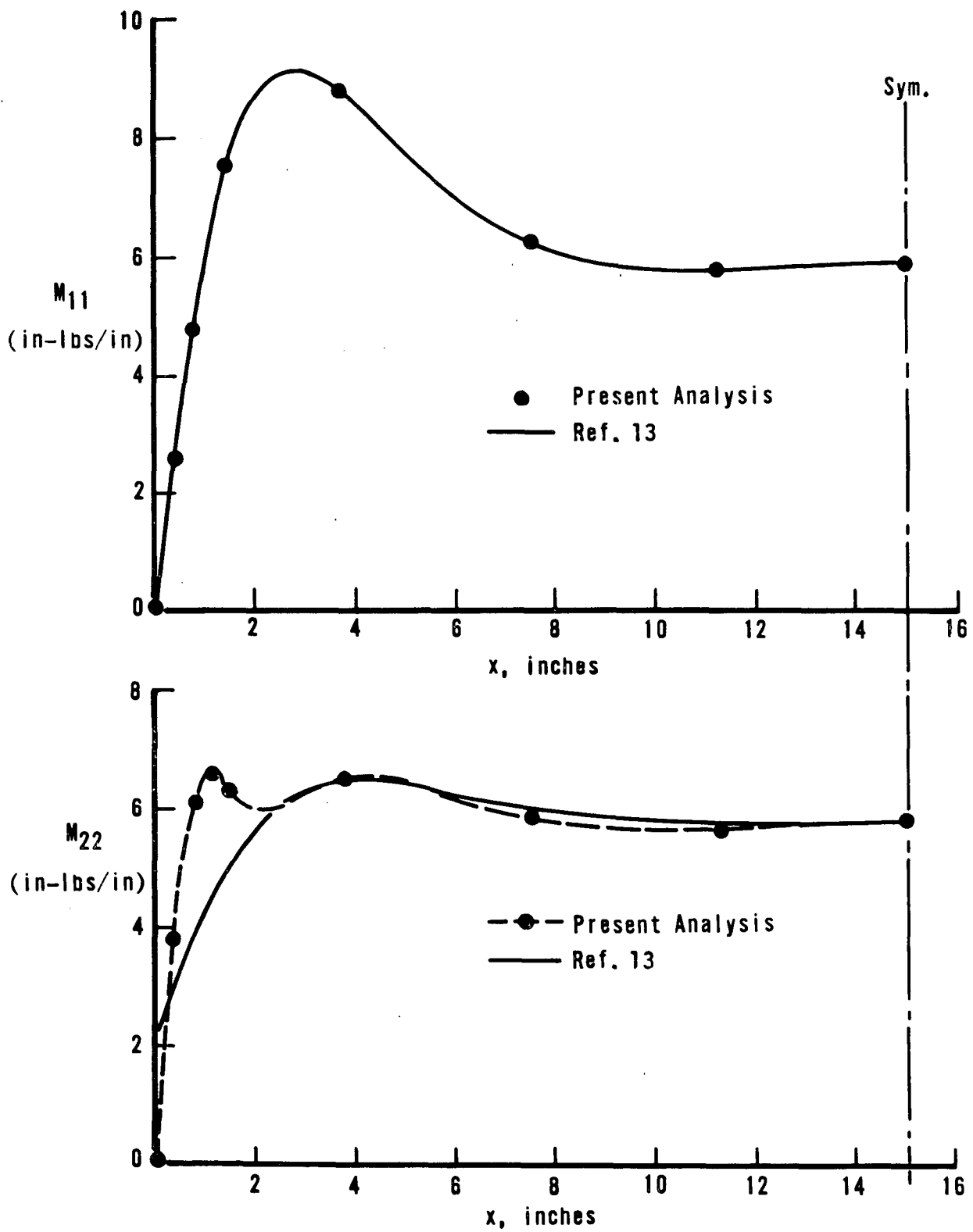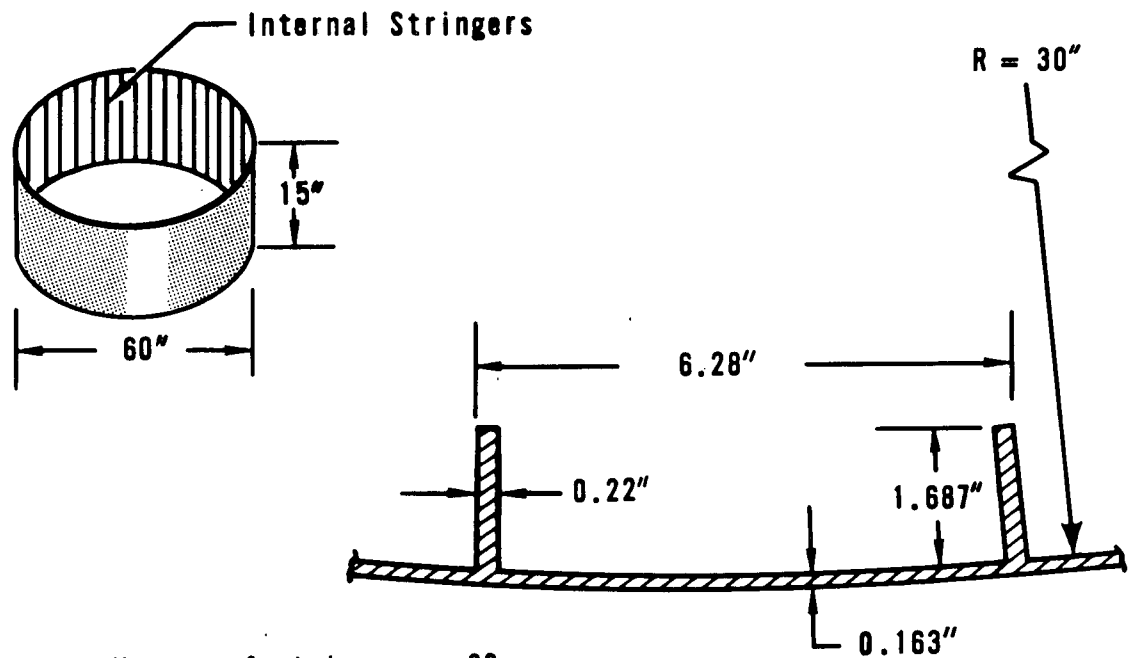
Number of stringers = 30

$\Delta T = 100°F$

Skin Properties:

$E_{11} = E_{22} = 10.5 \times 10^6$ lbs/in^2

$G_{12} = 3.98 \times 10^6$ lbs/in^2

$\nu_{12} = 0.32$

$\alpha_T = 14.0 \times 10^{-6}$ in/in/$°F$

Stringer Properties:

$GJ = 2.38 \times 10^4$ lbs/in^2

$I = 0.088$ in^4

$E = 10.5 \times 10^6$ lbs/in^2

$\alpha_T = 14.0 \times 10^{-6}$ in/in/$°F$

Figure 10. Stiffened Cylinder
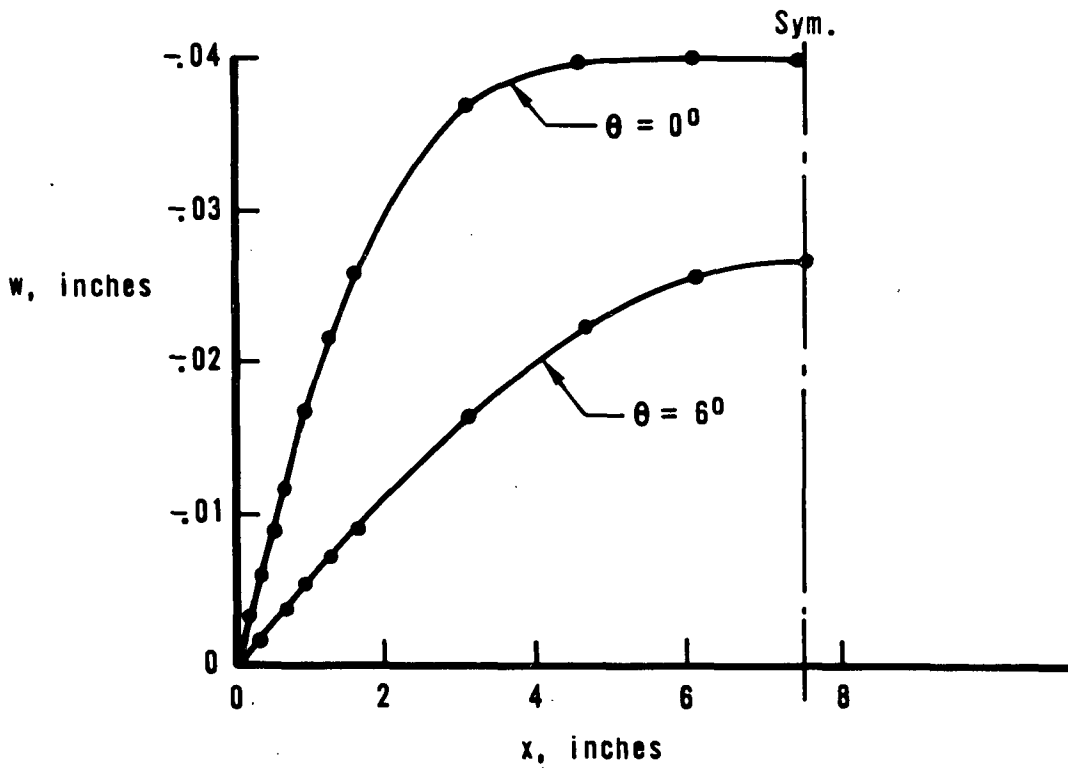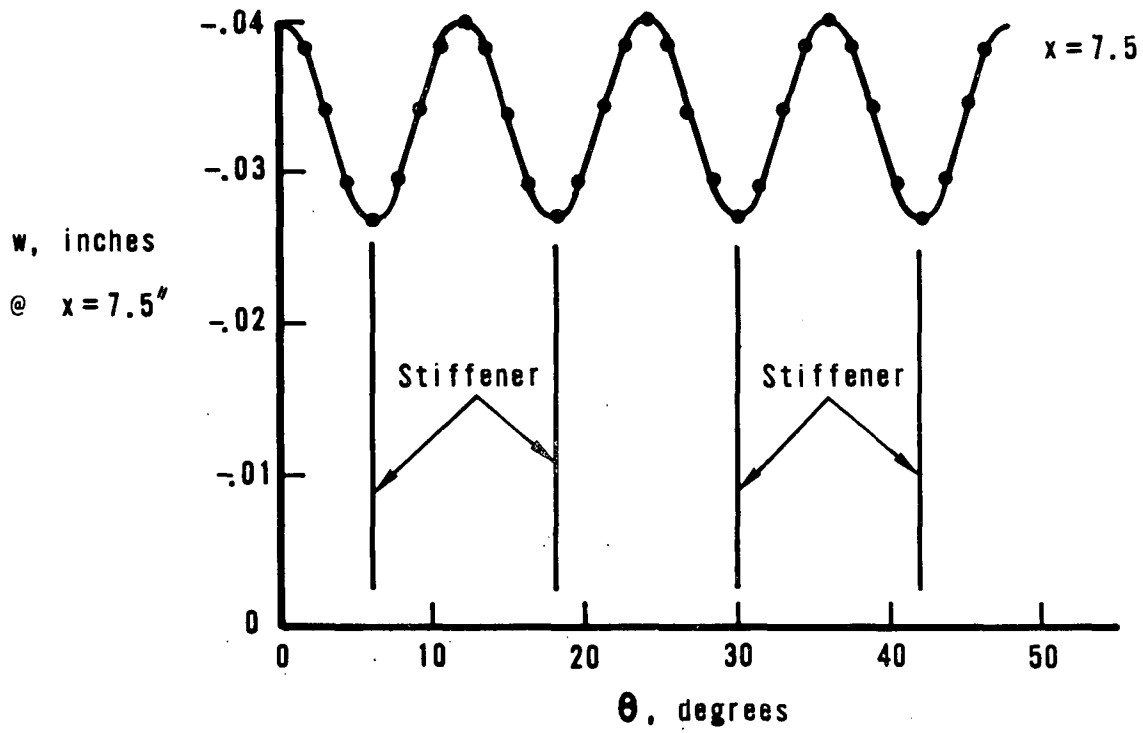
Figure 11. Integrally Stiffened Cylinder: Out-of-plane Thermal Displacements in the Shell Skin
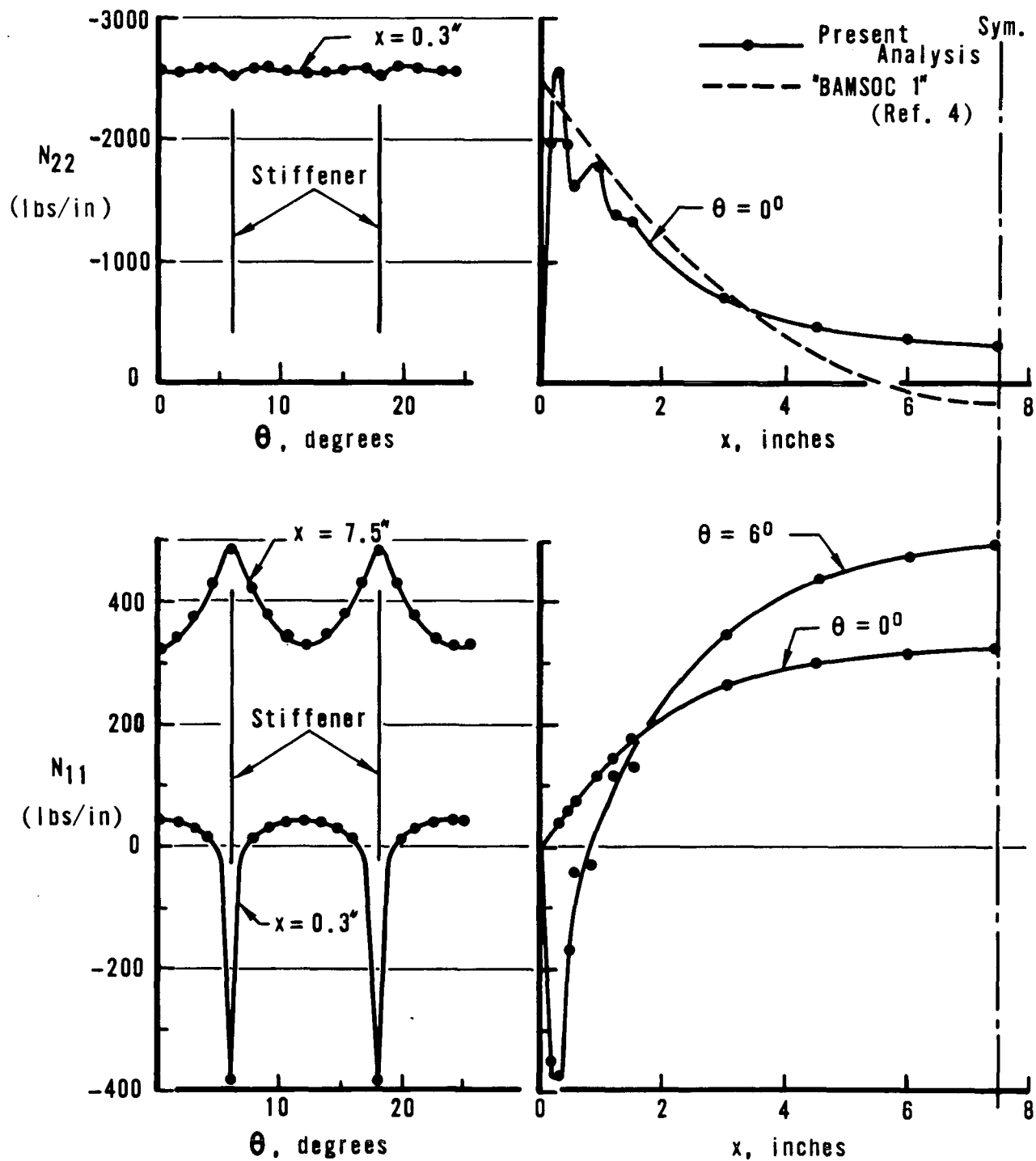
Figure 12.   Integrally Stiffened Cylinder: Thermal Stress in
the Shell Skin (1 of 2)
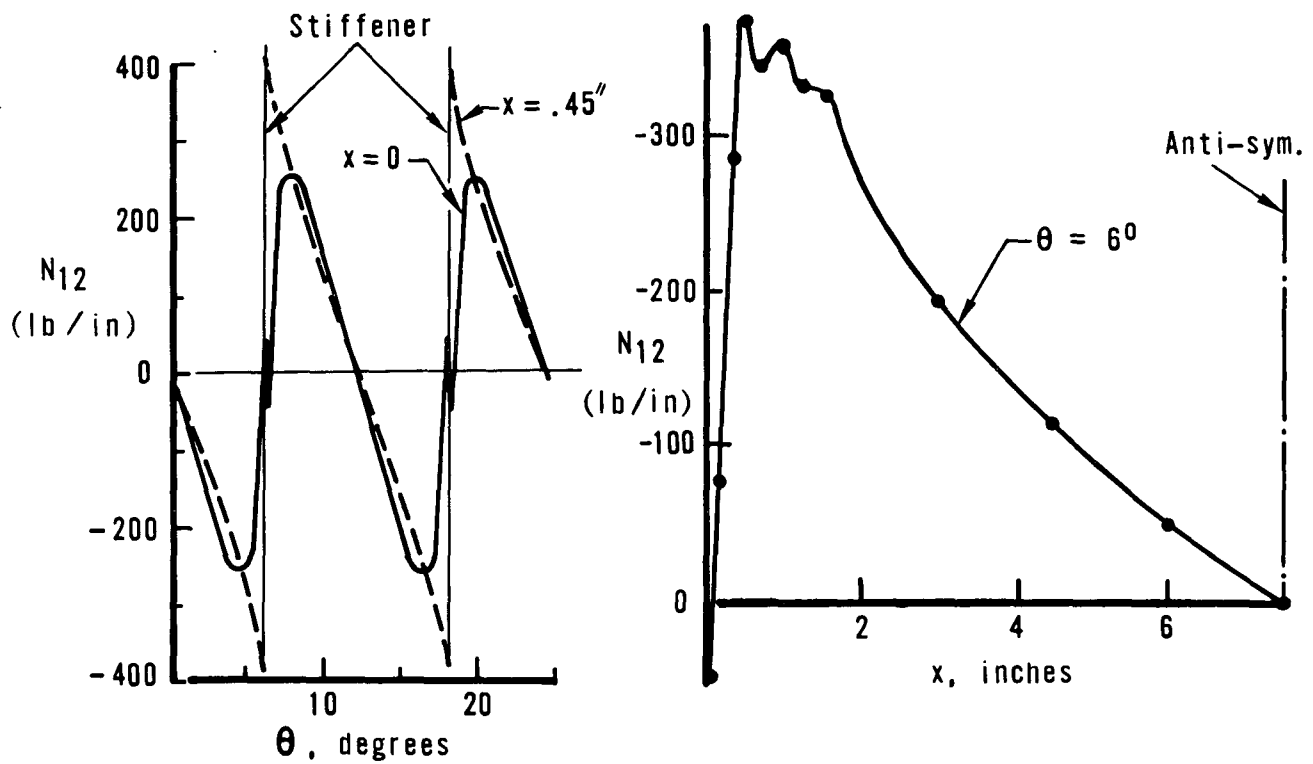
Figure 12. Integrally Stiffened Cylinder: Thermal Stress in the Shell Skin (2 of 2)
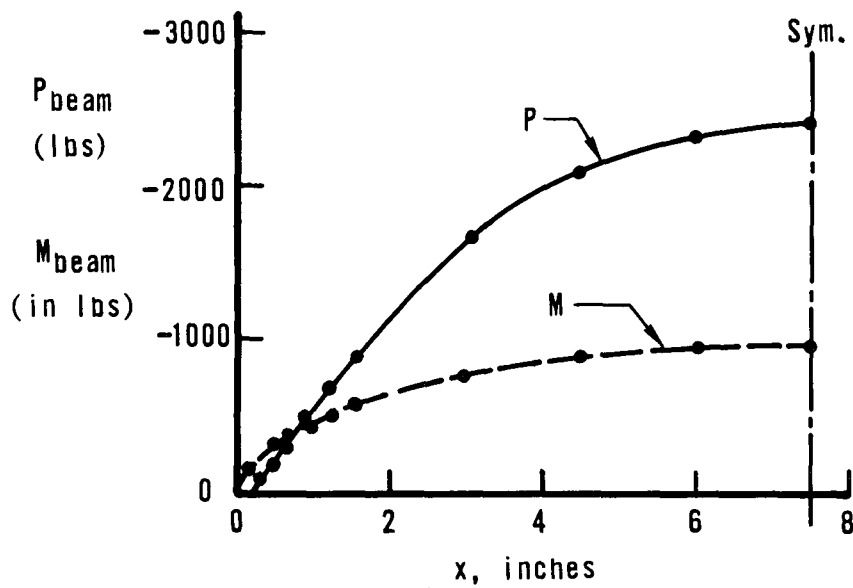
Figure 13. Integrally Stiffened Cylinder: Thermal Loads in the Stiffeners

Plates A and B

15″ 5″ t = 0.1 inch

x y

Simply Supported

15″ 10″

x y
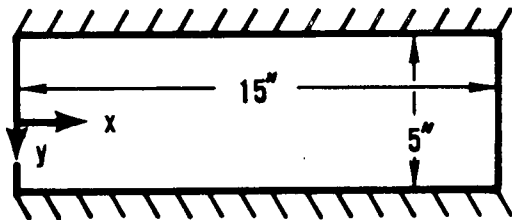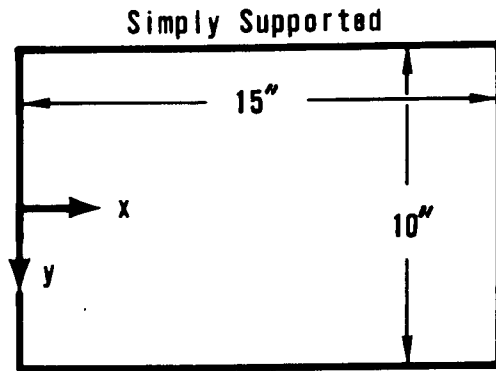
Simply Supported

t = 0.05 inch

Plates C and D

Material Properties

$E_{11} = E_{22} = 10.0 \times 10^6$ lbs/in^2

$G_{12} = 3.85 \times 10^6$ lbs/in^2

$\nu_{12} = 0.3$

$\alpha_T = 10 \times 10^{-6}$ in/in/^{0}F

Required Critical Loads

$\Delta T^0 F$

Plate A: $(\Delta T)_{cr}^0 F$

$\bar{N}_{11}$ $\Delta T = 35^0 F$ $\bar{N}_{11}$

Plate B: $(\bar{N}_{11})_{cr}$ lb /in

$\bar{N}_{11}$

Plate C: $(\bar{N}_{11})_{cr}$ lb/in

$\bar{N}_{11}$ $\bar{N}_0$
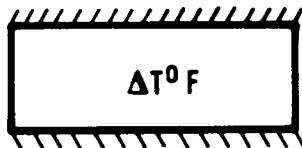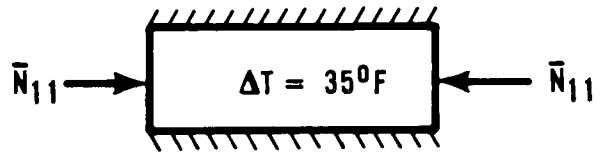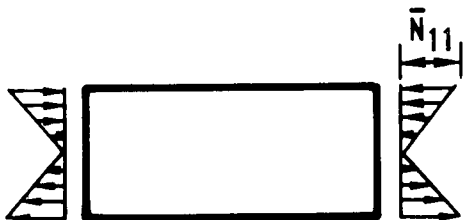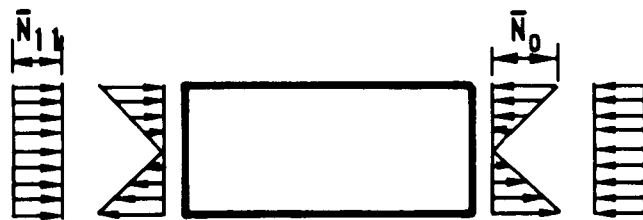
Plate D: $(\bar{N}_{11})_{cr}$ lb /in

$(\bar{N}_0 = 46.885$ lb/in$)$

Figure 14. Rectangular Flat Plates A to D
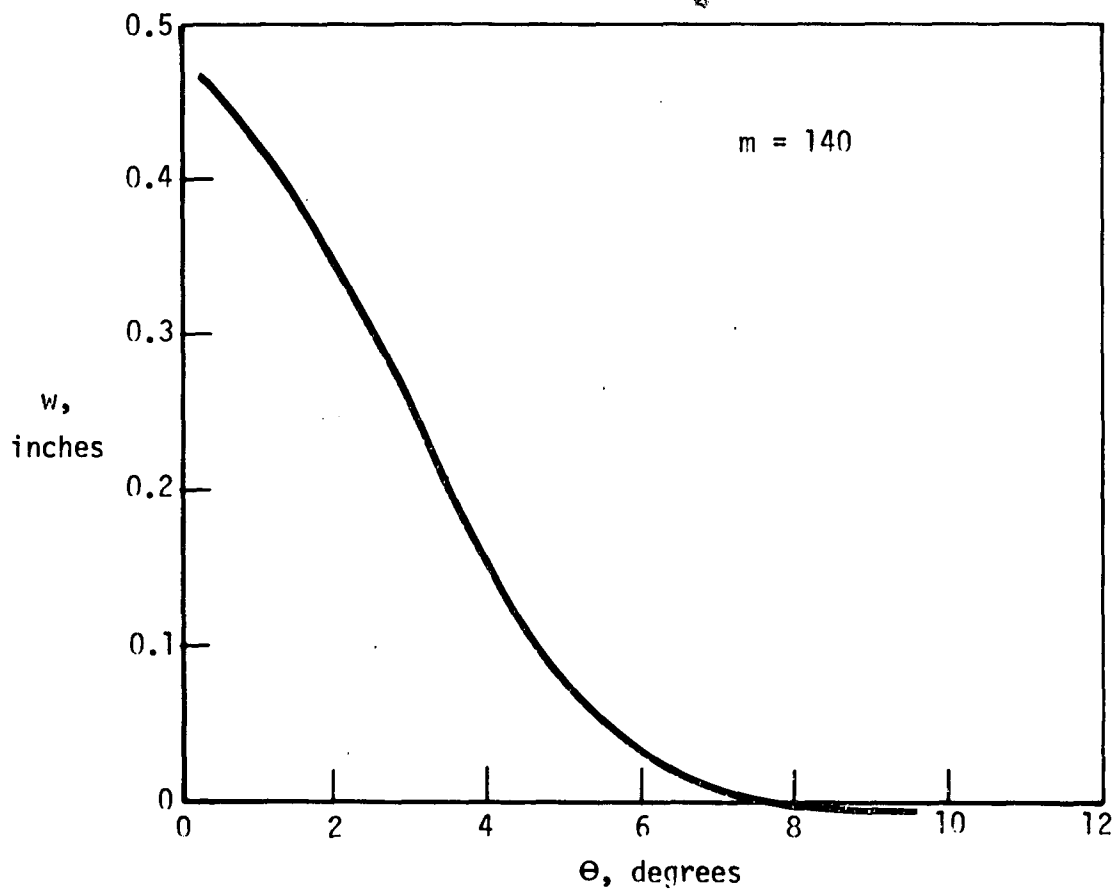
Figure 15   Buckling Mode Shape for Cylinder C
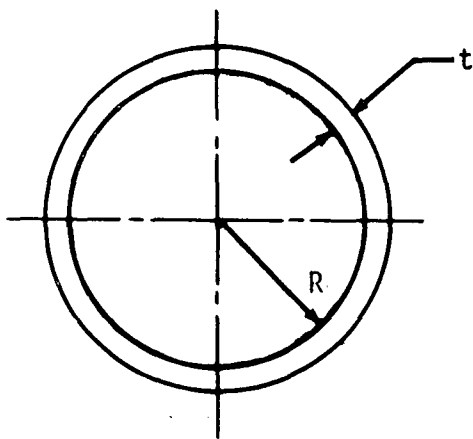
R   = 29.948 inches
t   = 0.1039 inches
Length = 94.25 inches

Material Properties:

$E_{11} = E_{22} = 10.0 \times 10^6$ lbs/in^2

G_{12} $= 4.286 \times 10^6$ lbs/in^2

ν_{12} $= 0.1667$

Figure 16   Geometry of Cylinder D

| m | Maximum Compressive Stress Resultant N_{11} (lb/in) | | |
	Present Analysis I*	Present Analysis II**	Ref. 18
1	2814.8	2999.7	2993.6
2	2609.9	2700.2	2690.1
3	2511.5	2571.5	2563.5
4	2453.7	2499.1	2489.5
5	2414.4	2451.2	2439.4
6	2390.8	2422.1	2402.3
7	2372.2	2399.2	2373.3
8	2351.1	2381.0	2349.7
9	2328.5	2349.6	2329.9

* Retainning all terms in equations (4.4) and (4.12) to (4.14)
** Dropping underlined terms in equations (4.4) and (4.12) to (4.14)
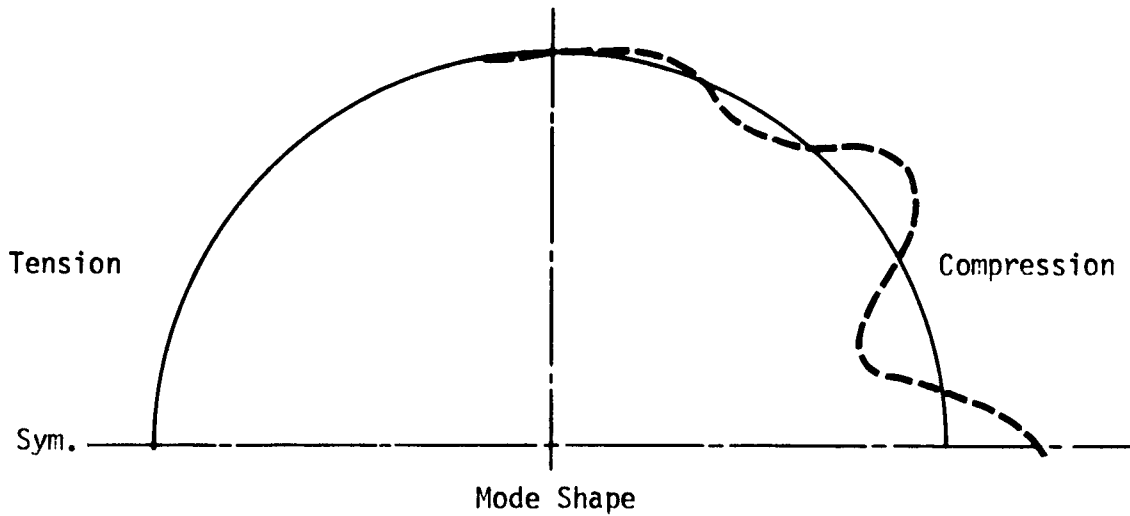
Figure 17   Results for Buckling of Cylinder D Under Pure Bending
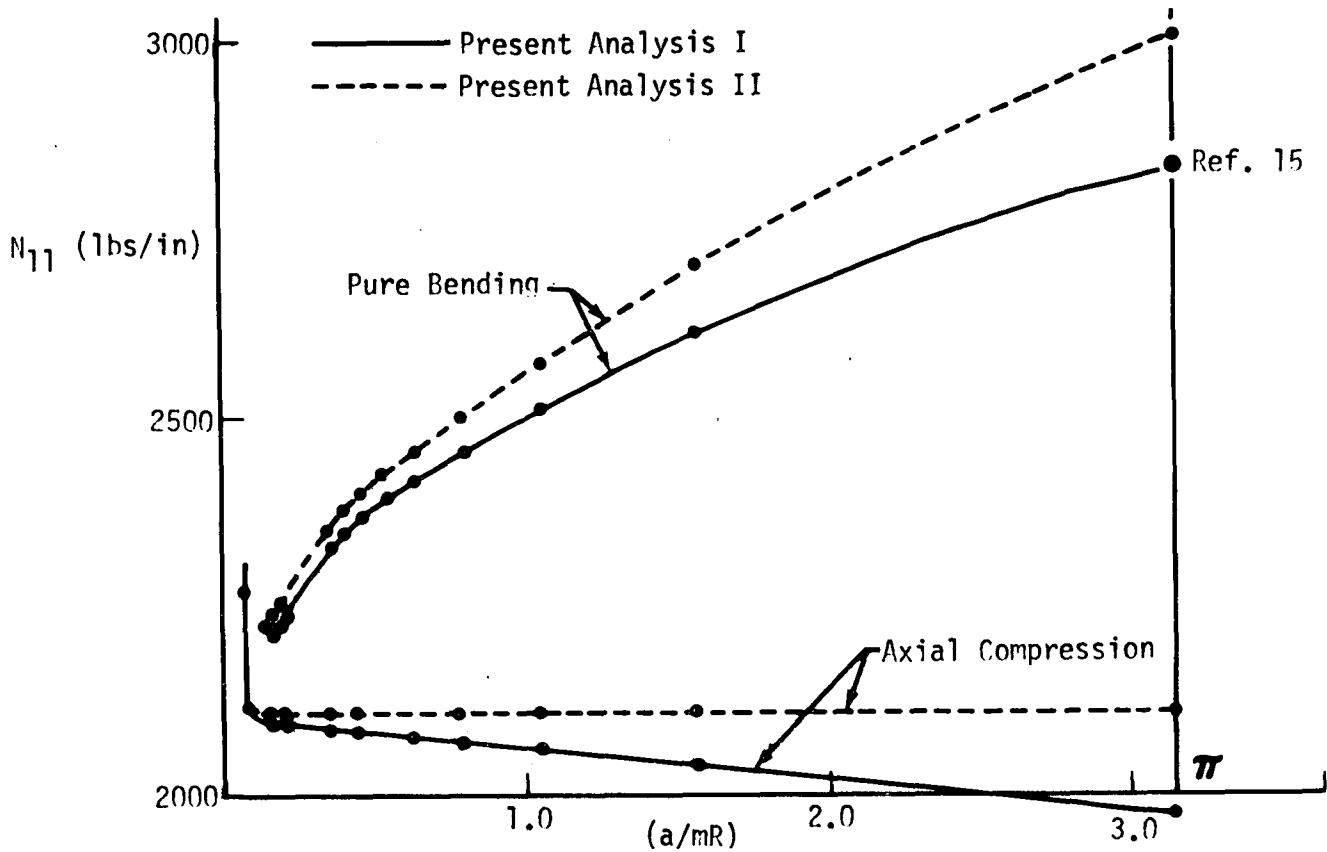
Present Analysis I retains all terms in equations (A.4) and (A.12) to (A.14)
Present Analysis II drops the underlined terms in the equations

Figure 18. Buckling of Cylinder D Under Pure Bending and
Under Axial Compression
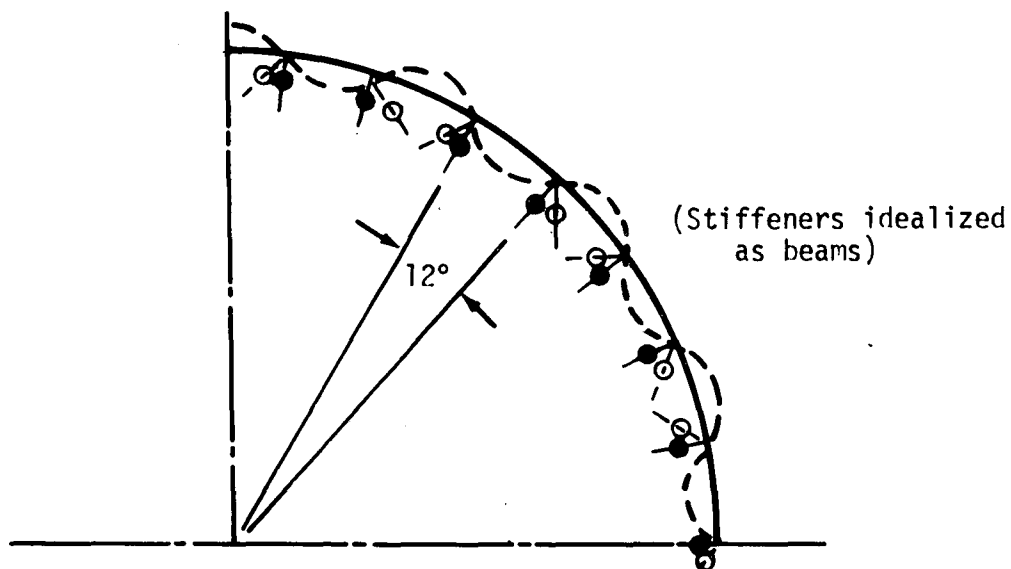
Figure 19. Mode Shape for Thermal Buckling of Stiffened
Cylinder (m = 1)
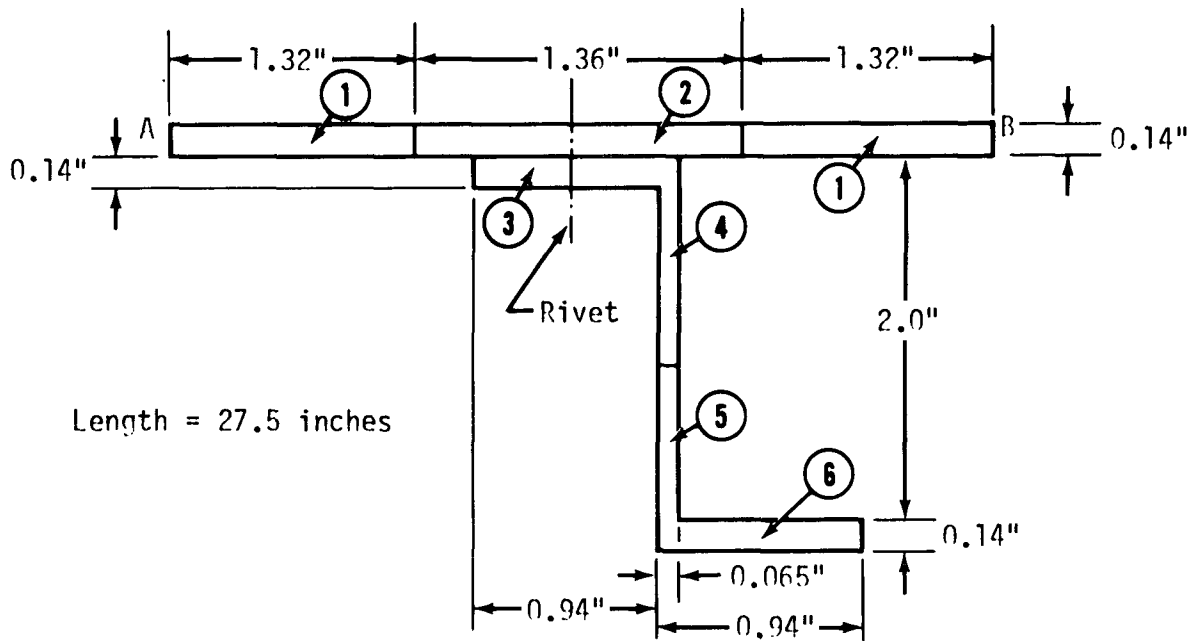
Segment No.	ΔT °F	$E_{11} \times 10^{-6}$ lbs/in^2	$\alpha_T \times 10^6$ in/in/°F	Thermal Stress N_{11} lbs/in
1	0	16.4	4.45	1020
2	80	16.1	4.50	189
3	100	16.0	4.52	-18
4	175	15.6	4.58	-373
5	250	15.2	4.65	-710
6	280	15.0	4.69	-1820

$$E_{11} = E_{22}$$

$$\nu_{12} = 0.3$$

$$G_{12} = \frac{E_{11}}{2(1 + \nu_{12})}$$

Figure 20 Heated Titanium Sheet-Stiffener Unit
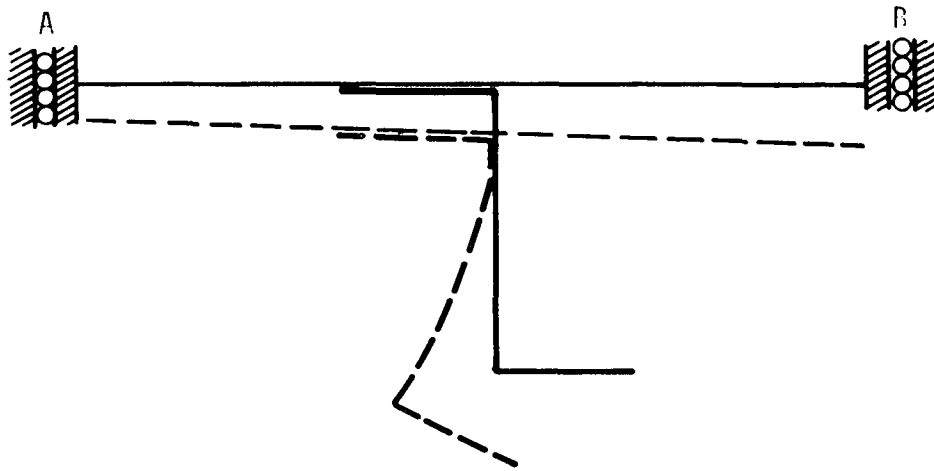
$$m \quad\quad = 1$$
$$P_{cr} \quad = 45515 \text{ lbs}$$
$$(\varepsilon_{11})_{cr} = 2.938 \times 10^{-3} \text{ in/in}$$
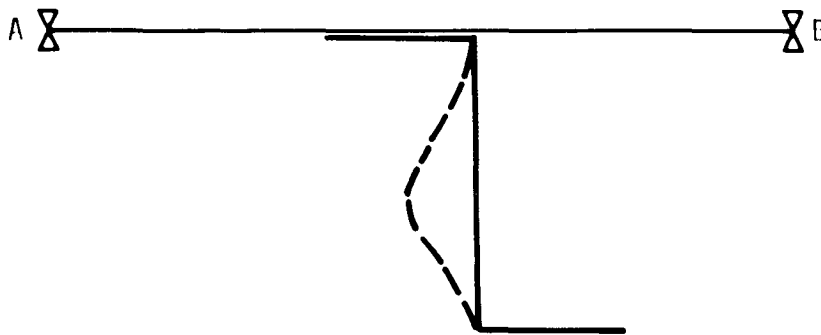
$$m \quad\quad = 18$$
$$P_{cr} \quad = 77145 \text{ lbs}$$
$$(\varepsilon_{11})_{cr} = 4.980 \times 10^{-3} \text{ in/in}$$

Figure 21 Buckling of a Heated Titanium Sheet-Stiffener Unit
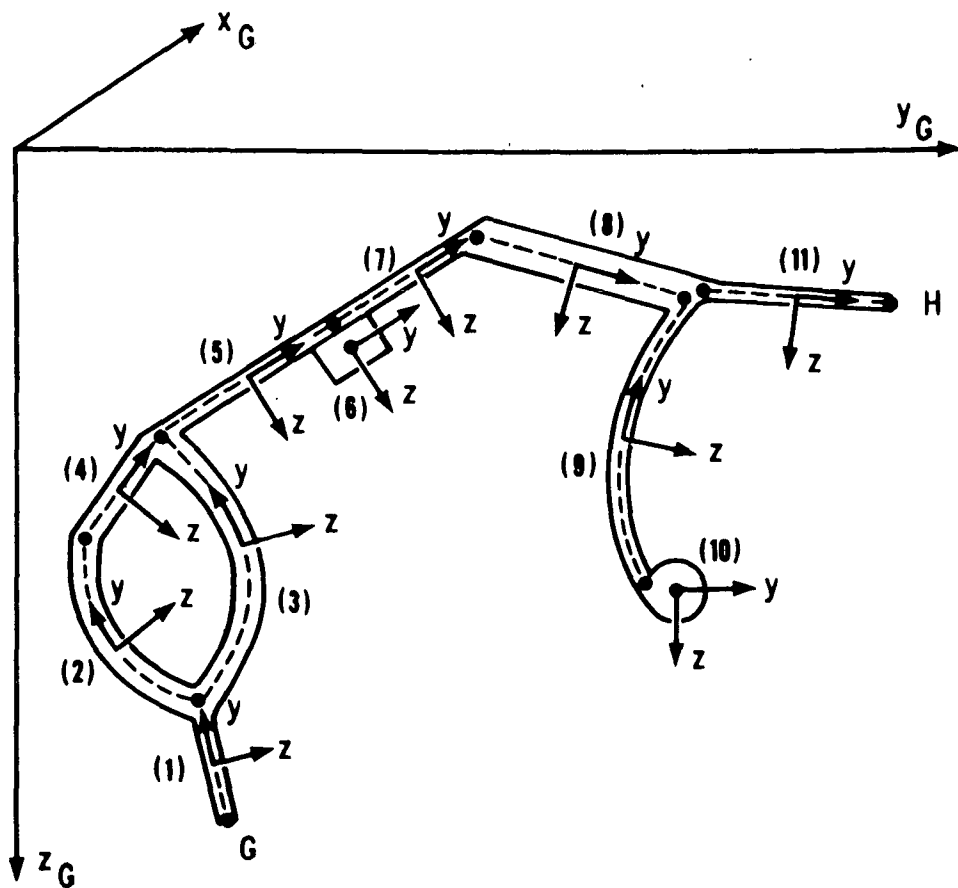
Figure 22. Idealization of an Arbitrary Structure
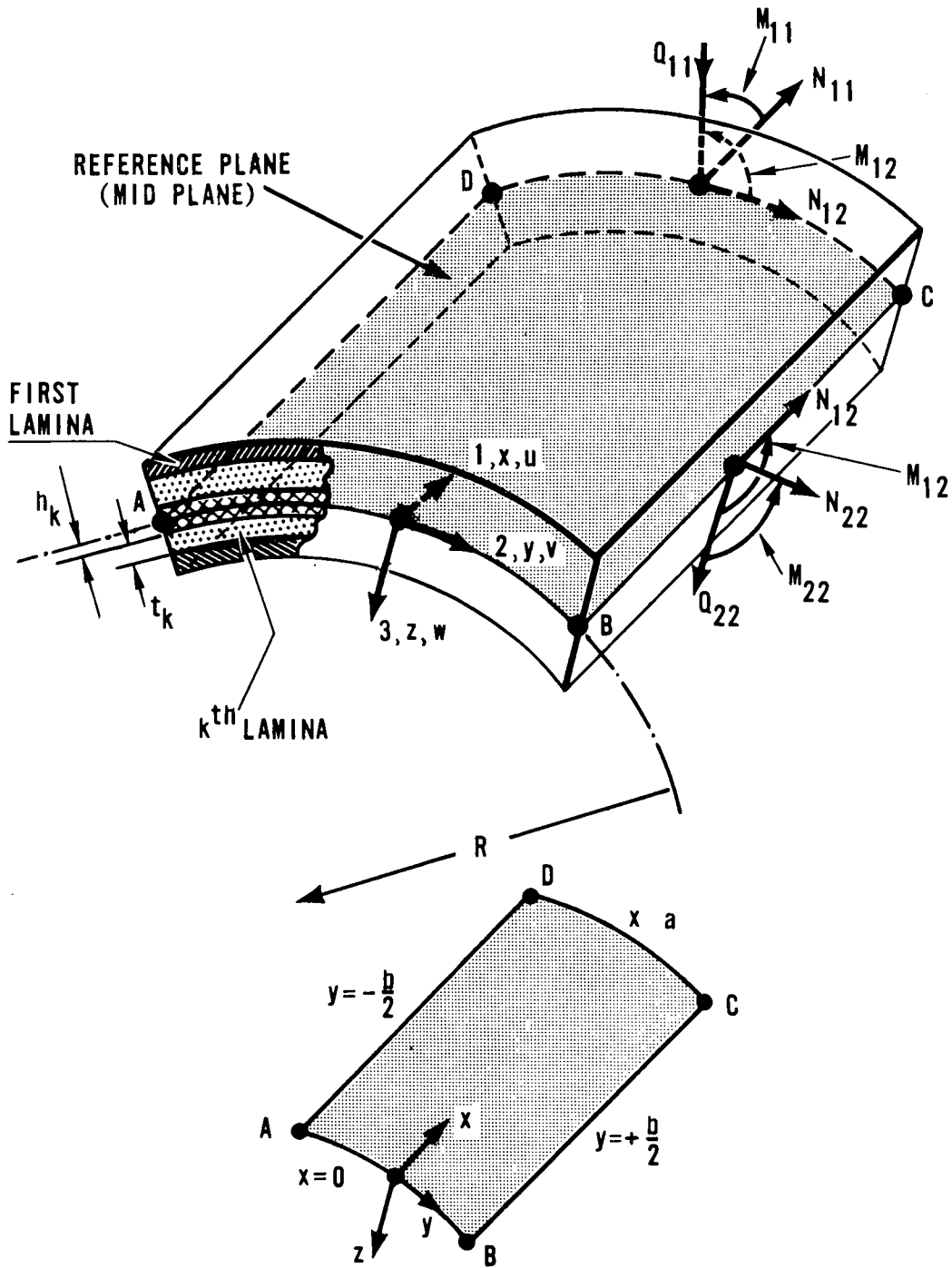
Figure 23. Laminated Plate-Strip Elements
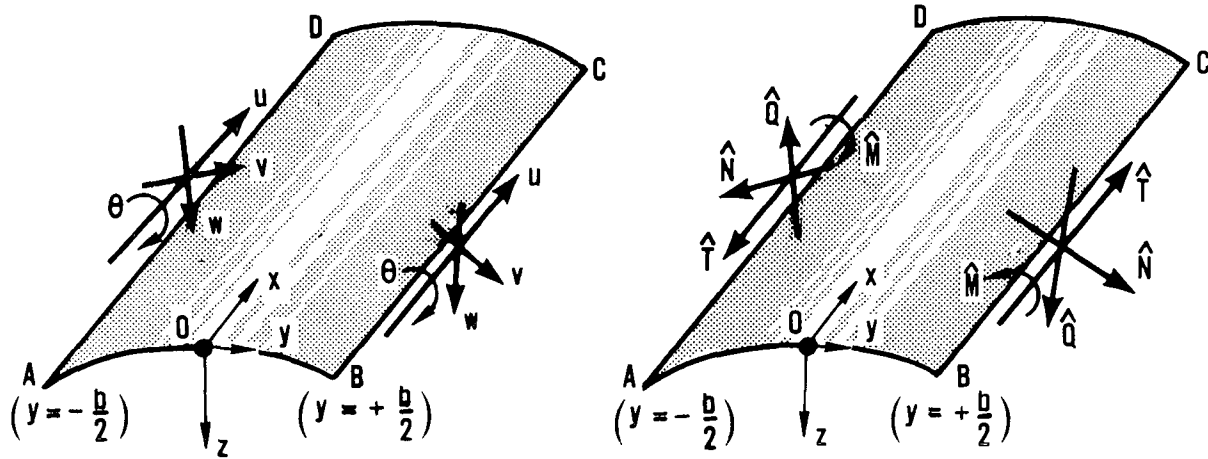
Figure 24.   Displacements and Forces Along the Sides of the
Plate-Strip Element
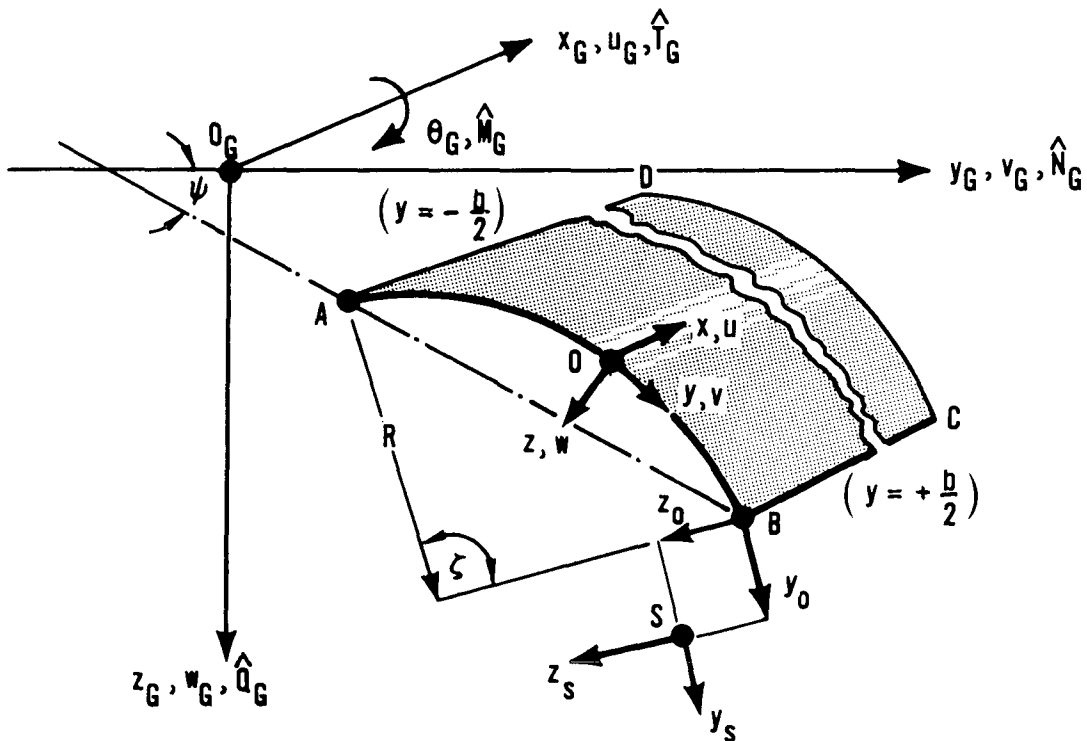
Figure 25.   Offsets and Global Axes for Plate-Strip Element

(a) Laminated Rectangular Beam

(b) Laminated Circular Beam

(c) Sign Conversions
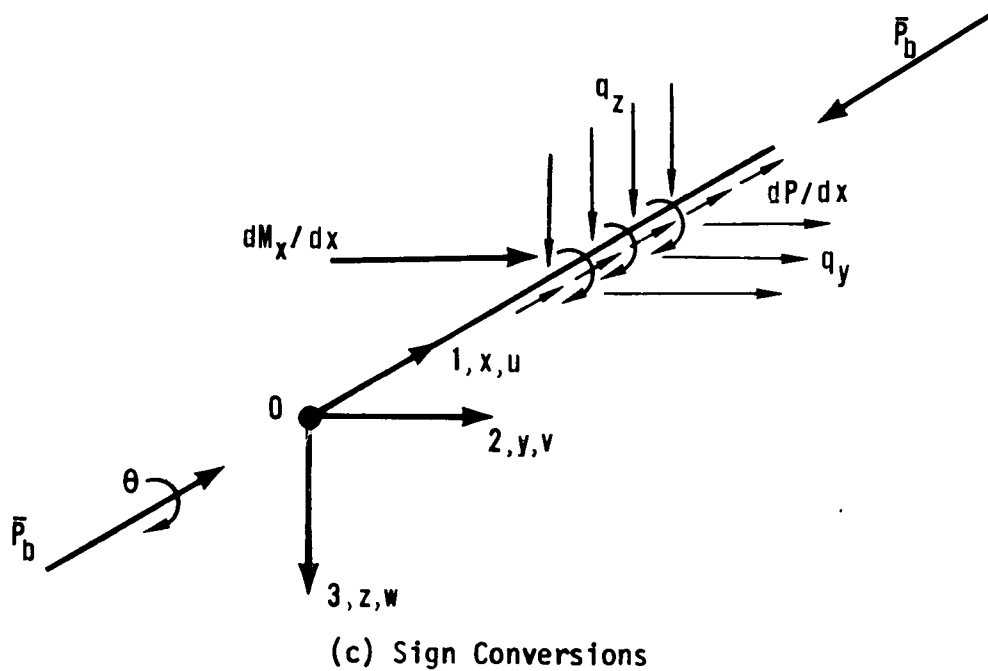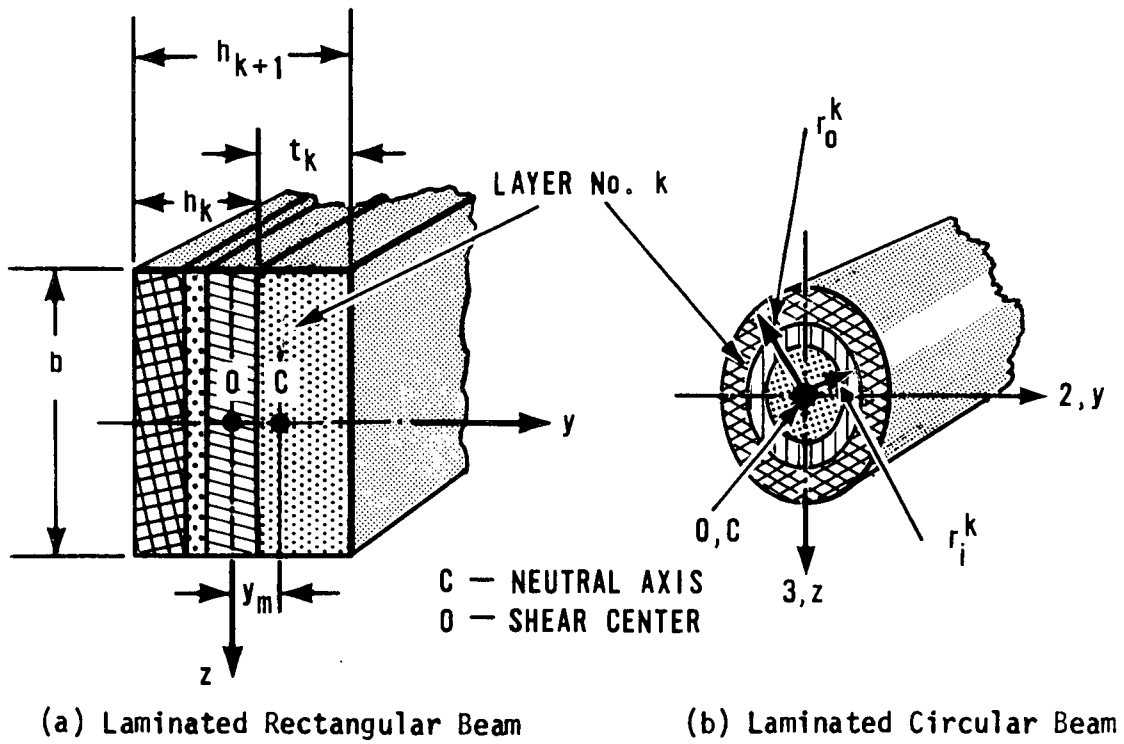
Figure 26. Beam Elements
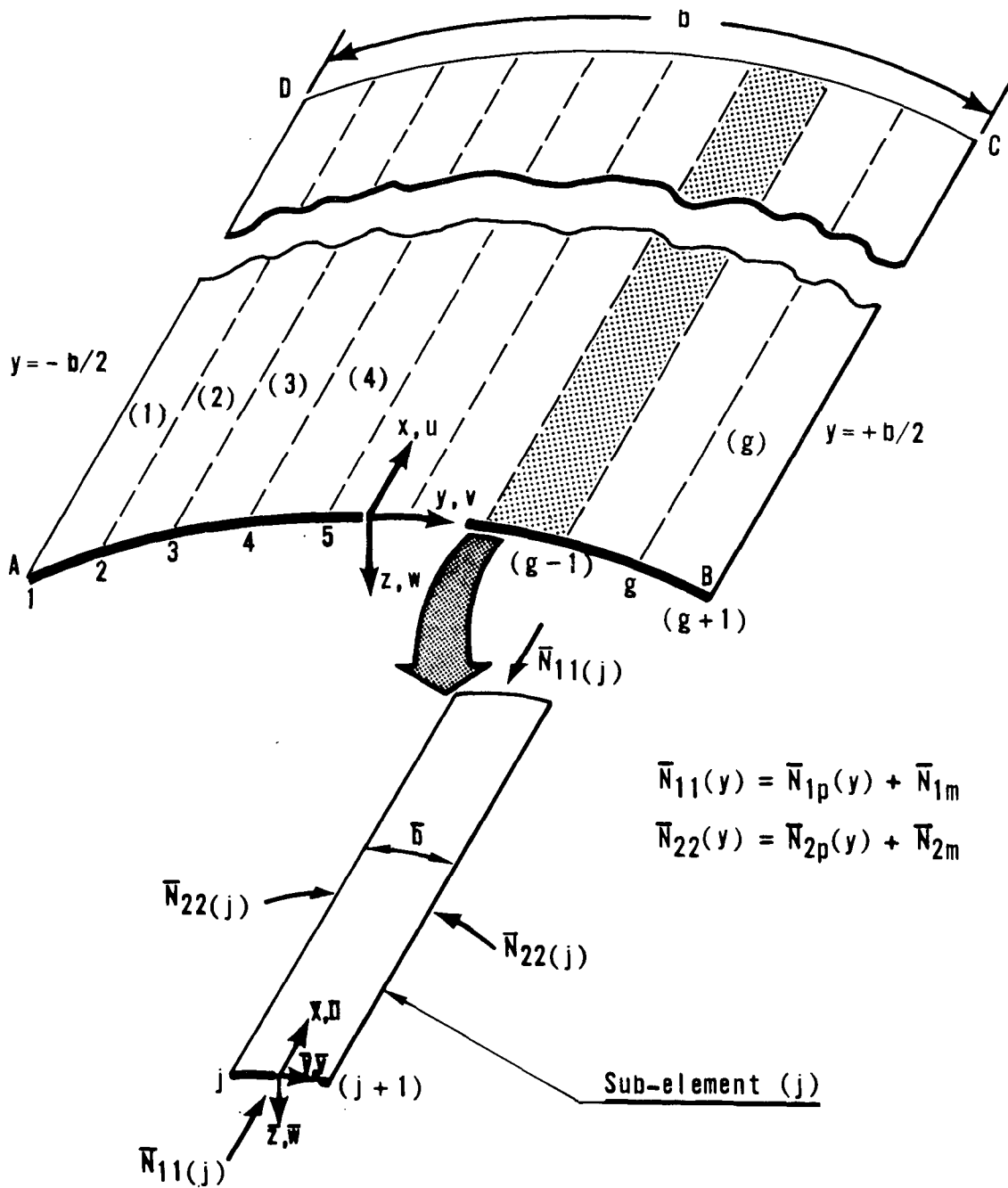
Figure 27. Sub-elements in Curved Plate-Strip Element

$$\overline{N}_{11}(y) = \overline{N}_{1p}(y) + \overline{N}_{1m}$$

$$\overline{N}_{22}(y) = \overline{N}_{2p}(y) + \overline{N}_{2m}$$

APPENDIX D

CONVERSION OF U.S. CUSTOMARY UNITS TO SI UNITS

The International System of Units (SI) was adopted by the Eleventh General Conference on Weights and Measures, Paris, October 1960, in Resolution No. 12. (See Ref. 27.) Conversion factors for the units used herein are given in the following tables:

Physical quantity	U.S. Customary Unit	Conversion factor (*)	SI Unit (**)
Area....................	in^2	6.452×10^{-4}	square meters (m^2)
Force..................	kip = 1000 lbf	4.448×10^3	newtons (N)
Length................	in.	2.54×10^{-2}	meters (m)
Moduli and stress......	ksi = 1000 lbf/in^2	6.895×10^6	newtons per square meter (N/m^2)
Stress resultant.......	lbf/in.	175.1	newtons per meter (N/m)
Temperature change.....	°F	5/9	Kelvin (K)

* Multiply value given in U.S. Customary Unit by conversion factor to obtain equivalent value in SI Unit.

** Prefixes to indicate multiple of units are as follows:

Prefix	Multiple
milli(m)	10^{-3}
centi(c)	10^{-2}
kilo(k)	10^3
giga(G)	10^9